NSI RRC KI 90-12/1-12-01

LWR MOX BENCHMARK CALCULATIONS USING THE BARS CODE PACKAGE

S.Akimushkin, A.Avvakumov, V.Malofeev, and A.Roslyakov

Date Published - December, 2001

NUCLEAR SAFETY INSTITUTE OF RUSSIAN RESEARCH CENTRE
''KURCHATOV INSTITUTE''
Kurchatov square 1
Moscow, Russia

ABSTRACT

This study was undertaken to validate the BARS code package for MOX-fuelled systems. Results for the pin cell validation of the TRIFON and UNK codes with a cross-section library based on ENDF/B-VI are presented. The pin power distributions within LWR MOX-fuelled cores were calculated by the BARS code and compared against measurements and other calculations. It was found that both TRIFON and UNK demonstrated a good agreement in calculations of the multiplication factor and the reactivity effects in the LWR MOX fuel cells. The BARS calculational results for the pin power distribution within LWR critical assemblies containing MOX fuel agree with high accuracy with the experimental results or calculations performed by precise methods.

TABLE OF CONTENTS

Page

ABSTRACT iii

LIST OF TABLES vii

LIST OF FIGURES ix

ACKNOWLEDGEMENTS xi

INTRODUCTION 1

References 3

1. LWR FUEL CELL CALCULATIONS 5

1.1. LWR Pin Cell Benchmark Intercomparison 5

1.2. OECD/NEA International Benchmark on Transmutation Concepts 11

1.3 VVER Calculational Benchmark 21

1.4. Benchmark Calculations of Power Distribution within Fuel Assemblies 33

Discussions 40

References 41

2. LWR CORE CALCULATIONS 43

2.1. PNL MOX Assemblies 43

2.2. Saxton MOX Assemblies 49

2.3. TCA MOX Assemblies 54

2.4. ESADA MOX Assemblies 59

2.5. KRITZ Reactor Series 63

2.6. UO_2-MOX Core Calculational Benchmark 69

Discussions 75

References 76

CONCLUSIONS 79

References 81

LIST OF TABLES

Table		Page
1.1.	Fuel Number Densities (10^{-24} cm^{-3}) for Standard PWR Lattice	5
1.2.	Cladding and Moderator Number Densities (10^{-24} cm^{-3})	5
1.3.	Fuel, Cladding and Moderator Temperatures (K)	6
1.4.	Comparison of K_{inf} Calculational Results for UOX Cells	7
1.5.	Comparison for Reactivity Effects (pcm) in UOX Cells	7
1.6.	Comparison of K_{inf} Calculational Results for MOX Cells	8
1.7.	Comparison for Doppler Effect (pcm) in MOX Cells (Cases 1 – 2)	8
1.8.	Neutron Balance Comparison for UOX Case 1	9
1.9.	Neutron Balance Comparison for MOX Case 1	9
1.10.	Fuel Number Densities (10^{-24} cm^{-3}) for Standard PWR Lattice	11
1.11.	Fuel Number Densities (10^{-24} cm^{-3}) for Highly Moderated PWR Lattice	12
1.12.	Cladding and Moderator Number Densities (10^{-24} cm^{-3})	12
1.13.	Comparison of Calculational Results for MOX12 Case (Standard Lattice)	14
1.14.	Comparison of Calculational Results for MOX22 Case (Standard Lattice)	15
1.15.	Comparison of Calculational Results for MOX22 Case (Highly Moderated Lattice)	16
1.16.	Averaged Values (with One Standard Deviation)	17
1.17.	State Parameters of Cells	21
1.18.	Fuel Material Composition for Variants	22
1.19.	Non-fuel Material Composition	23
1.20.	Comparison of K_{inf} Calculational Results for UOX Cell V1	24
1.21.	Comparison for Reactivity Effects (pcm) in UOX Cell V1	24
1.22.	Comparison of K_{inf} Calculational Results for MOX Cell V2	25
1.23.	Comparison for Reactivity Effects (pcm) in MOX Cell V2	25
1.24.	Comparison of K_{inf} Calculational Results for MOX Cell V7	26
1.25.	Comparison for Reactivity Effects (pcm) in MOX Cell V7	26
1.26.	Comparison of K_{inf} Calculational Results for MOX Cell V8	27
1.27.	Comparison for Reactivity Effects (pcm) in MOX Cell V8	27
1.28.	Comparison of K_{inf} Calculational Results for MOX Cell V9	28
1.29.	Comparison for Reactivity Effects (pcm) in MOX Cell V9	28
1.30.	Comparison of K_{inf} Calculational Results for MOX Cell V10	29

1.31. Comparison for Reactivity Effects (pcm) in MOX Cell V10 29
1.32. Neutron Balance Comparison for UOX Case V1S1 30
1.33. Neutron Balance Comparison for MOX Case V2S1 30
1.34. Fuel Number Densities (10^{-24} cm^{-3}) 33
1.35. Cladding and Moderator Number Densities (10^{-24} cm^{-3}) 33
1.36. Comparison of K_{inf} Calculational Results 34
1.37. Deviations of K_{inf} (pcm) from the Mean Values 35
1.38. Neutron Balance Comparison for UOX Fuel 35
1.39. Neutron Balance Comparison for MOX 4.3% 36
1.40. Neutron Balance Comparison for MOX 7.0% 37
1.41. Neutron Balance Comparison for MOX 8.7% 38
2.1. Parameters of PNL Assemblies 43
2.2. K_{eff} Calculational Results for PNL MOX Assemblies 46
2.3. RMS Deviations (%) from Measured Data in Pin-Power Distribution 47
2.4. RMS Deviations (%) from the KENO-V Data in Pin-Power Distribution 47
2.5. Parameters of Selected Single-Region Assemblies 49
2.6. K_{eff} Calculational Results for Saxton Assemblies 52
2.7. RMS Deviations (%) from the KENO-V Data in Pin-Power Distribution 52
2.8. Parameters of TCA Assemblies 54
2.9. K_{eff} Calculational Results for TCA Assemblies (Part I) 56
2.10. K_{eff} Calculational Results for TCA Assemblies (Part II) 57
2.11. RMS Deviations (%) from the KENO-V Data in Pin-Power Distribution 57
2.12. Parameters of ESADA Assemblies 60
2.13. K_{eff} Calculational Results for ESADA Assemblies 62
2.14. Parameters of KRITZ Cores 63
2.15. K_{eff} Calculational Results for KRITZ Cores 65
2.16. RMS Deviations (%) from the Measured Pin-Power Distribution 65
2.17. Comparison of Calculational Results 72
2.18. RMS Deviations (%) in Pin-Power Distribution 73

LIST OF FIGURES

Figure		Page
1.1.	Void Effect for MOX12 Case (Standard Lattice) vs. Void Fraction	18
1.2.	Void Effect for MOX22 Case (Standard Lattice) vs. Void Fraction	19
1.3.	Void Effect for MOX22 Case (Highly Moderated Lattice) vs. Void Fraction	20
2.1.	Configurations of MOX Assemblies PNL-30 through PNL-32	44
2.2.	Configurations of MOX Assemblies PNL-33 through PNL-35	45
2.3.	Pin-Power Distributions for PNL Assemblies	48
2.4.	Configurations of MOX Assemblies SAXTON-1 through SAXTON-6	51
2.5.	Pin-Power Distributions for SAXTON-2	53
2.6.	Configurations of TCA Lattices Types	55
2.7.	Pin-Power Distributions for TCA-3, TCA-5, and TCA-10	58
2.8.	Some Configurations of ESADA Lattice Types	61
2.9.	Configurations of KRITZ Cores	64
2.10.	Pin-Power Distributions for KRITZ Core 2:1	66
2.11.	Pin-Power Distributions for KRITZ Core 2:13	67
2.12.	Pin-Power Distributions for KRITZ Core 2:19	68
2.13.	Geometry of UO_2 and MOX Assemblies	70
2.14.	Geometry of UO_2-MOX Core	71
2.15.	Comparison of Pin-Power Distributions	74

ACKNOWLEDGEMENTS

The authors would like to thank Drs. V.Tsybulsky and V.Davidenko (RRC KI, Russia) who provided the UNK code and an expanded version of the ENDF/B-VI based library.
The authors wish to thank Dr. D.J.Diamond (BNL, USA) for his help in providing the data for the validation.

INTRODUCTION

Development of MOX fuel begun since the end of the fifties. Now several countries reuse MOX fuel recovered from spent fuel, but within no more than 30% of the total core loading. Many years of operational experience (more than 150 reactor-years) with MOX-fuelled cores along with well-developed technologies in the management of MOX fuel demonstrate possibilities in extending MOX fuel share in commercial nuclear power plants.

However, it is obvious that large-scale use of MOX fuel in commercial reactors will demand new approaches to confirm the LWR operational regimes in which MOX fuels comply with safety criteria. It is known that changes in isotopic and spectral characteristics of MOX fuel compared with conventional UO_2 fuel results in lower boron and control rod worth and more negative fuel (Doppler) and moderator temperature coefficients. In this respect a problem of improvements in approaches for modeling MOX cores becomes essential. Consequently, there is a need to validate calculational procedures for physics modeling of MOX-fuelled cores against the measurements and precise calculations.

Nowadays the most of modern computing tools used for the LWR in-core management and safety analysis, consist in two stages. First stage is a preparation of the cross-section sets on the basis of the up-to-date evaluated nuclear data files, such as, for instance, JEF-2.2, ENDF/B-V, ENDF/B-VI, and JENDL-3.2. As a rule, these sets are generated for the whole fuel assembly and for this reason must be calculated by a 2-D code. Second stage consists in global 3-D core calculations using, therefore, an assembly-by-assembly approach. That is why it is necessary to validate neutronic calculational methods for both the database generation and the core calculation.

Unlike widely spread assembly-by-assembly approach in the core calculation, the BARS code package is based on a pin-by-pin approach [1]. The neutronic database is calculated for the separate pin cell and, thus, allows taking into account intra-assembly effects within each assembly. This advantage becomes valuable because of a modern LWR MOX fuel assembly has very complicated composition.

Previously, the comprehensive validation of the BARS code package was undertaken [1-4]. This validation dealt with conventional UO_2 fuels at wide range of burnup, but did not include MOX fuel. It was found that approaches implemented in the BARS code package, met all demands on the calculational accuracy to predict the basic neutronic parameters of LWRs: the multiplication factor, the fuel temperature effects, the void and moderator temperature effects, and the spatial pin power effects.

This report is focused on the BARS code package validation for MOX-fuelled systems. All calculational results were obtained using the neutron databases generated on the basis of the nuclear evaluated file ENDF/B-VI by either the TRIFON or UNK codes. A problem with a resonance treatment for U and Pu nuclides is very important. TRIFON allows to take into account explicitly only few most strong resonances, the rest are treated using effective resonance levels (totally about 500 groups). Unlike TRIFON, the UNK code allow to use a fine energy group structure for more correct representation of the resonance regions (totally about 10,000 groups). Brief descriptions of these codes are given in previous verification reports [2, 3]. Note that both codes used the same initial multigroup database prepared by the NJOY code [5]. Recently, this database as well as both codes were improved to extend their capabilities in calculation of MOX fuel.

Section 1 of the report contains a comparison the calculational results obtained by different codes using various cross-sections for LWR MOX pin cells. A pin cell consists of fuel pellet, clad, and moderator regions with using neutron reflection condition at the outer boundary of the cell. The pin cell is the simplest approach to calculate LWR lattice and allows to compare different neutron databases generated by using various nuclear data libraries, as well as, spectrum computing techniques, without influence of spatial effects (due to neutron leakage). Such pin cell may be considered as a model of infinite fuel lattice, and, therefore, allows to investigate only asymptotic spectrum within fuel lattice. This drawback may be overcome by considering next approximation - a multicell model which takes into account not only intra-assemly effects, but also the complicated spectrum at the boundary between UO_2 and MOX fuels. In Section 1 four pin cell benchmarks were analyzed: three of them in square geometry used in western LWRs and one – in triangular geometry used in Russian VVERs. The following safety related parameters were investigated: the multiplication factor, neutron balance, and the reactivity effects. The last effects include the fuel temperature (Doppler) effects, the void and moderator temperature effects, and the boron and Xe/Sm poisoning effects.

Section 2 focuses on spatial pin power effects within rather simple MOX-fuelled cores of LWR type. Here both the experimental and numerical benchmark cores were investigated. Five experimental benchmarks included PNL, Saxton, TCA, ESADA, and KRITZ cores with different configurations. The effective multiplication factor and power distribution inside the core were compared with the measurements and calculational results obtained by using different codes.

References

1. A. Avvakumov, V. Malofeev, “Validation of a Pin-by-Pin Neutron Kinetics Method for LWRs,” Proceeding of the International Twenty-Sixth Water Reactor Safety Information Meeting, Bethesda, Maryland, October 1998
2. A. Avvakumov and V. Malofeev, “An Advanced 3 D Pin-by-Pin Neutronic Model for the LWR RIA Analysis: Features, Advantages and Validation,” Report No. 90-12/1-8-97, Nuclear Safety Institute of Russian Research Centre “Kurchatov Institute”, 1997
3. A. Avvakumov, et al., “Validation of the BARS Code Package with ENDF/B Based Data Library,” Report No. 90-12/1-4-98, Nuclear Safety Institute of Russian Research Centre “Kurchatov Institute”, 1998
4. A. Avvakumov, V. Malofeev, and V. Sidorov, “Analysis of Pin-by-Pin Effects for LWR Rod Ejection Accident,” NUREG/IA-0175, NSI RRC KI 90-12/1-3-00, IPSN/00-13, 2000
5. R.E. McFarlane, “NJOY91.91: A Code System for Producing Pointwise and Multigroup Neutron and Photon Cross Sections from ENDF/B Evaluated Nuclear Data,” ORNL PSR-171, Oak Ridge National Laboratory, 1993

1. LWR FUEL CELL CALCULATIONS

1.1. LWR Pin Cell Benchmark Intercomparison

Calculations for simple LWR pin cell models fuelled with uranium oxide (UOX) or mixed uranium/plutonium oxide (MOX) have been performed by different codes with using different nuclear data libraries [1,2]. Four cases were investigated for UOX cells: Case 1 – the reference one at 293 K; Case 2 – with reduced water density; Case 3 – with increase in fuel temperature from 550 to 900 K (compared to Case 4) and Case 4 – with isothermal temperature increase from 293 to 550 K). Two cases (with two fuel temperatures: 300 and 560 K) and with two different MOX fuel compositions (MOX-1 and MOX-2) were considered for MOX cells. In all cases neutron leakage was zero.

The nuclide number densities and temperatures for different cases are presented in Tables 1.1-1.3. The fuel and cladding radii are 0.4 and 0.45 cm; outer cell radius is 0.6770275 cm (1.2-cm lattice pitch) for UOX fuel and 0.710879 cm (1.26-cm lattice pitch) for MOX fuel.

Table 1.1. Fuel Number Densities (10^{-24} cm^{-3}) for Standard PWR Lattice

Nuclide	UOX fuel	MOX-1 fuel	MOX-2 fuel
^{235}U	7.0803 –4*	5.105 –5	5.118 –5
^{238}U	2.2604 –2	2.037 -2	2.042 -2
^{238}Pu	-	4.669 –5	2.714 –5
^{239}Pu	-	1.465 -3	1.972 -3
^{240}Pu	-	5.691 -4	4.256 -4
^{241}Pu	-	2.713 -4	3.577 –5
^{242}Pu	-	1.413 -4	1.234 –5
^{241}Am	-	3.028 -5	1.406 -5
O	4.6624 -2	4.588 -2	4.588 -2

* Read as 7.0803×10^{-4}

Table 1.2. Cladding and Moderator Number Densities (10^{-24} cm^{-3})

Zone	Nuclide	UOX (Case 1)	UOX (Cases 2-4)	MOX
Cladding	Zr	4.3241 -2*	4.3241 -2	3.880 -2
Moderator	H	6.6988 -2	4.6892 -2	4.744 -2
	O	3.3414 -2	2.3390 -2	2.372 -2

* Read as 4.3241×10^{-2}

Table 1.3. Fuel, Cladding and Moderator Temperatures (K)

Zone	UOX (Cases 1-2)	UOX (Case 3)	UOX (Case 4)	MOX (Case 1)	MOX (Case 2)
Fuel	293	900	550	300	560
Cladding	293	600	550	300	300
Moderator	293	550	550	300	300

The following effects of reactivity were investigated:

- the fuel temperature (Doppler) effect for UOX and MOX cells;
- the coolant temperature and density effects for UOX cells.

In the current comparison with the UNK and TRIFON calculations, 12 (for UOX cells) and 11 (for MOX cells) sets of calculational data were used [1,2]. Two continuos-energy Monte-Carlo codes (MCNP-4A and TRIPOLI-4) and six deterministic cell codes (RESMOD, ECCO, APOLLO-2.4.1, LWR-WIMS, WIMSD-5A and SCALE-4.2/XSDRNPM) were considered in [1]. Results in [2] were obtained using the same SCALE/XSDRN and RESMOD together with two Monte-Carlo codes: continuos-energy MCNP-4B and group KENO-VI. Only results calculated in cylindrical zero-leakage cell geometry were used in the current comparison. All participants [1,2] used nuclear cross-sections data derived from the JEF-2.2 library. The UNK and TRIFON calculations were performed using nuclear cross-sections based on the ENDF/B-VI library.

Calculational results are summarized in Tables 1.4-1.7. Reactivity effects are determined as differences between multiplication factors (K_{inf}) of the different cases and given in units of pcm (10^{-5}). At the bottom of tables there are the mean values of parameter of interest with one standard deviation (σ). Deviations of the calculated effects from the mean value are also included in Tables 1.5 and 1.7 in brackets.

Comparison of neutron balances calculated by different codes for UOX and MOX cells (Case 1) is shown in Tables 1.8-1.9 (with total neutron absorption normalized to 10^5). Besides, there are data on three-group neutron balances [1] but it is impossible to use them in the current intercomparison because the energy group boundaries do not coincide with those used in TRIFON and UNK.

Table 1.4. Comparison of K_{inf} Calculational Results for UOX Cells

	Case 1	Case 2	Case 3	Case 4
MCNP-4A	1.38774	1.33452	1.30309	1.31492
TRIPOLI-4	1.38805	1.33585	1.30246	1.31539
RESMOD [1]	1.38884	1.33685	1.30476	1.31985
ECCO	1.38750	1.33515	1.30265	1.31770
APOLLO-2.4.1	1.38735	1.33452	1.30224	1.31696
LWR-WIMS	1.38797	1.33783	1.30519	1.32014
WIMSD-5A	1.38411	1.33166	1.29828	1.31362
XSDRN [1]	1.38526	1.33366	1.30059	1.31623
MCNP-4B	1.3865	1.3336	1.3030	1.3164
KENO-VI	1.3856	1.3327	1.2995	1.3145
RESMOD [2]	1.3894	1.3374	1.3057	1.3199
XSDRN [2]	1.3851	1.3326	1.2997	1.3145
TRIFON	1.38501	1.33275	1.30012	1.31501
UNK	1.38672	1.33346	1.30364	1.31733
Mean value	1.38680 ± 0.00153	1.33447 ± 0.00185	1.30221 ± 0.00219	1.31660 ± 0.00208

Table 1.5. Comparison for Reactivity Effects (pcm) in UOX Cells

	Cases 1 - 2	Cases 2 - 4	Cases 4 - 3	Cases 2 - 3	Cases 1 - 3
MCNP-4A	5322 (89)	1960 (174)	1183 (-256)	3143 (-83)	8465 (6)
TRIPOLI-4	5220 (-13)	2046 (260)	1293 (-146)	3339 (113)	8559 (100)
RESMOD [1]	5199 (-34)	1700 (-86)	1509 (70)	3209 (-17)	8408 (-51)
ECCO	5235 (2)	1745 (-41)	1505 (66)	3250 (24)	8485 (26)
APOLLO-2.4.1	5283 (50)	1756 (-30)	1472 (33)	3228 (2)	8511 (52)
LWR-WIMS	5014 (-219)	1769 (-17)	1495 (56)	3264 (38)	8278 (-181)
WIMSD-5A	5245 (12)	1804 (18)	1534 (95)	3338 (112)	8583 (124)
XSDRN [1]	5160 (-73)	1743 (-43)	1564 (125)	3307 (81)	8467 (8)
MCNP-4B	5290 (57)	1720 (-66)	1340 (-99)	3060 (-166)	8350 (-109)
KENO-VI	5290 (57)	1820 (34)	1500 (61)	3320 (94)	8610 (151)
RESMOD [2]	5200 (-33)	1750 (-36)	1420 (-19)	3170 (-56)	8370 (-89)
XSDRN [2]	5250 (17)	1810 (24)	1480 (41)	3290 (64)	8540 (81)
TRIFON	5226 (-7)	1775 (-12)	1489 (49)	3264 (38)	8489 (31)
UNK	5326 (93)	1613 (-173)	1369 (-70)	2982 (-244)	8308 (-151)
Mean value	5233 ± 76	1786 ± 103	1439 ± 103	3226 ± 102	8459 ± 99

Table 1.6. Comparison of K_{inf} Calculational Results for MOX Cells

	MOX-1		MOX-2	
	Case 1	Case 2	Case 1	Case 2
MCNP-4A	1.21840	1.20048	1.26106	1.24564
TRIPOLI-4	1.21902	1.20407	1.26233	1.24830
RESMOD [1]	1.22065	1.20660	1.26370	1.24950
ECCO	1.22335	1.20885	1.26419	1.25033
APOLLO-2.4.1	1.21817	1.20316	1.26019	1.24609
LWR-WIMS	1.21656	1.20371	1.25862	1.24510
XSDRN [1]	1.22238	1.20763	1.26465	1.25057
MCNP-4B	1.2200	1.2054	1.2621	1.2484
KENO-VI	1.2160	1.2010	1.2593	1.2459
RESMOD [2]	1.2189	1.2048	1.2631	1.2498
XSDRN [2]	1.2155	1.2011	1.2593	1.2456
TRIFON	1.22630	1.21122	1.26644	1.25220
UNK	1.22098	1.20670	1.26061	1.24735
Mean value	1.21971 ± 0.00295	1.20498 ± 0.00308	1.26197 ± 0.00228	1.24806 ± 0.00221

Table 1.7. Comparison for Doppler Effect (pcm) in MOX Cells (Cases 1 – 2)

	MOX-1	MOX-2
MCNP-4A	1792 (319)	1542 (151)
TRIPOLI-4	1495 (22)	1403 (12)
RESMOD [1]	1405 (-68)	1420 (29)
ECCO	1450 (-23)	1386 (-5)
APOLLO-2.4.1	1501 (28)	1410 (19)
LWR-WIMS	1285 (-188)	1352 (-39)
XSDRN [1]	1475 (2)	1408 (17)
MCNP-4B	1460 (-13)	1370 (-21)
KENO-VI	1500 (27)	1340 (-51)
RESMOD [2]	1410 (-63)	1330 (-61)
XSDRN [2]	1440 (-33)	1370 (-21)
TRIFON	1509 (36)	1424 (33)
UNK	1428 (-45)	1326 (-65)
Mean value	1473 ± 108	1391 ± 54

Table 1.8. Neutron Balance Comparison for UOX Case 1

		MCNP-4A	ECCO	APOLLO	TRIFON	UNK
^{235}U	Fission	53 722	53 727	53 711	53 587	53 592
	Capture	10 902	10 896	10 949	11 036	11 037
	Absorption	64 624	64 623	64 660	64 623	64 629
^{238}U	Fission	2 780	2 775	2 768	2 837	2 848
	Capture	25 844	25 851	25 825	25 746	25 746
	Absorption	28 624	28 626	28 593	28 583	28 594
Zr	Capture	650	647	653	674	679
H+O	Capture	6 101	6 105	6 092	6 120	6 098

Table 1.9. Neutron Balance Comparison for MOX Case 1

		MCNP-4A	TRIFON	UNK
^{235}U	Fission	720	760	715
	Capture	259	289	271
	Absorption	979	1 050	986
^{238}U	Fission	3 041	3 048	3 167
	Capture	18 735	18 961	18 678
	Absorption	21 776	22 009	21 846
^{238}Pu	Fission	109	105	105
	Capture	408	437	418
	Absorption	517	542	522
^{239}Pu	Fission	29 812	29 874	29 798
	Capture	16 003	15 441	16 070
	Absorption	45 815	45 315	45 868
^{240}Pu	Fission	481	463	470
	Capture	14 976	14 766	14 817
	Absorption	15 457	15 228	15 287
^{241}Pu	Fission	7 942	8 173	7 921
	Capture	2 426	2 371	2 330
	Absorption	10 368	10 544	10 252
^{242}Pu	Fission	90	90	91
	Capture	2 008	2 026	1 992
	Absorption	2 098	2 116	2 083
^{241}Am	Fission	29	30	30
	Capture	1 246	1 268	1 200
	Absorption	1 275	1 298	1 230
Zr	Capture	552	572	584
H+O	Capture	1 337	1 326	1 340

Analysis of the calculated results for the UOX cells presented in Table 1.4, shows that all codes calculates the multiplication factor within $\pm 1.8\sigma$. This corresponds to 0.2–0.3% uncertainty in K_{inf}. It should be noted that the APOLLO-2.4.1 and MCNP-4B results are very close to the mean values (deviation in K_{inf} is less than 0.07%). Reactivity effects are predicted with very good accuracy (see Table 1.5) with two exceptions: MCNP-4A and TRIPOLI-4 in Cases 2 – 4 and 4 – 3. May be these are due to insufficient statistic histories in Monte-Carlo calculations. Nevertheless, excluding these results it should be concluded that the moderator density (Cases 1 – 2) and total (Cases 1 – 3) effects are estimated with about 5% uncertainty, and the rest temperature effects – with about 10% uncertainty.

For the MOX fuel cells a standard deviation in K_{inf} reaches 0.2–0.25% (see Table 1.6). The TRIFON code gives the highest values of K_{inf} with 0.3–0.5% overestimation, and MCNP-4B gives only 0.03% deviation from the mean value. On the other hand, all codes (except for MCNP-4A) estimate the Doppler reactivity effect with high accuracy. If do not take into account the MCNP-4A results (deviations are about 3σ) and the LWR-WIMS result for MOX-1, the rest results are within no more than 100 pcm or 7%.

It is important to pay attention to the results obtained by the same codes RESMOD and XSDRN from [1] and [2]. All of them used cross-sections obtained from the same JEF-2.2 library. Comparison shows that there are large differences (500–700 pcm) in the XSDRN results for K_{inf} in the MOX cases. The maximum difference in the Doppler effects for the UOX and MOX fuel cells is about 6.5%. These seem to be due to different options of codes and different ways in generating cross-sections.

Comparison of the neutron balance from Table 1.8 shows that for UOX Case 1 the process rates are in excellent agreement except for Zr capture rate (it seems to be due to different self-shielding factors in JEF-2.2 and ENDF/B-VI). For MOX Case 1 as shown in Table 1.9, 0.4% difference in K_{inf} between TRIFON and UNK is mainly due to differences in ^{239}Pu fission and capture rates. On the other hand, the process rates for major important nuclides are in rather good agreement.

1.2. OECD/NEA International Benchmark on Transmutation Concepts

In the framework of OECD/NEA NSC project on different transmutation concepts, calculations of an MOX-PWR benchmark have been performed to investigate uncertainties in the basic physics parameters: multiplication factor, the Doppler and void effects [3,4]. This benchmark is based on a standard PWR cell (moderator-to-fuel volume ratio: V_m/V_f = 1.929) and a wide cell (V_m/V_f = 3.0) for the highly moderated PWR. Two plutonium and minor actinide (MA) compositions were considered. These are denoted as MOX12 and MOX22 and represent recycled MOX fuel compositions with burnups of 33 and 50 GWd/t. For the highly moderated PWR lattice, only the MOX22 case was adopted. In addition, the total MA contents are 0.0, 1.0 and 2.5 wt.% respectively. In the framework of the current comparison, only initial states (at the beginning of cycle) were used. The nuclide number densities are presented in Tables 1.10-1.12. The fuel and cladding radii are 0.4095 and 0.475 cm; outer cell radius is 0.741 cm for the standard PWR lattice and 0.8536 cm for the highly moderated PWR lattice. These correspond to lattice pitches of 1.3133 and 1.513 cm respectively. Fuel temperatures are 660 and 960°C; moderator/cladding temperature is 306.3°C.

Table 1.10. Fuel Number Densities (10^{-24} cm^{-3}) for Standard PWR Lattice

	MOX12 (33 GWd/tHM)			MOX22 (50 GWd/tHM)		
	0.0% MA	1.0% MA	2.5% MA	0.0% MA	1.0% MA	2.5% MA
^{235}U	4.6618 -5*	4.4263 -5	4.1190 -5	1.4144 -4	1.3547 -4	1.2639 -4
^{238}U	2.0673 -2	1.9628 -2	1.8265 -2	1.9752 -2	1.8918 -2	1.7651 -2
^{237}Np	-	1.0332 -5	2.5881 -5	-	1.0105 -5	2.5357 -5
^{238}Pu	5.6777 -5	7.8873 -5	1.0646 -4	1.2477 -4	1.5081 -4	1.9044 -4
^{239}Pu	9.7176 -4	1.3499 -3	1.8222 -3	1.2751 -3	1.5412 -3	1.9462 -3
^{240}Pu	6.7695 -4	9.4041 -4	1.2694 -3	9.2817 -4	1.1219 -3	1.4167 -3
^{241}Pu	2.3366 -4	3.2459 -4	4.3814 -4	3.1953 -4	3.8622 -4	4.8771 -4
^{242}Pu	2.0745 -4	2.8819 -4	3.8900 -4	3.4388 -4	4.1564 -4	5.2487 -4
^{241}Am	3.7123 -5	1.4349 -4	3.5946 -4	5.1734 -5	1.3366 -4	3.3540 -4
^{243}Am	-	5.5790 -5	1.3976 -4	-	5.9941 -5	1.5041 -4
^{244}Cm	-	1.9974 -5	5.0037 -5	-	2.5952 -5	6.5121 -5
O	4.5807 -2	4.5768 -2	4.5813 -2	4.5873 -2	4.5798 -2	4.5839 -2

* Read as 4.6618×10^{-5}

Table 1.11. Fuel Number Densities (10^{-24} cm^{-3}) for Highly Moderated PWR Lattice

	MOX22 (50 GWd/tHM)		
	0.0% MA	1.0% MA	2.5% MA
^{235}U	1.4994 -4*	1.4400 -4	1.3317 -4
^{238}U	2.0939 -2	2.0109 -2	1.8596 -2
^{237}Np	-	1.0084 -5	2.5286 -5
^{238}Pu	7.3785 -5	9.9693 -5	1.4991 -4
^{239}Pu	7.5405 -4	1.0188 -3	1.5320 -3
^{240}Pu	5.4889 -4	7.4162 -4	1.1152 -3
^{241}Pu	1.8896 -4	2.5531 -4	3.8392 -4
^{242}Pu	2.0336 -4	2.7476 -4	4.1317 -4
^{241}Am	3.0594 -5	1.3339 -4	3.3446 -4
^{243}Am	-	5.9819 -5	1.4999 -4
^{244}Cm	-	2.5899 -5	6.4939 -5
O	4.5873 -2	4.5798 -2	4.5839 -2

* Read as 1.4994×10^{-4}

Table 1.12. Cladding and Moderator Number Densities (10^{-24} cm^{-3})

Zone	Nuclide	Number Densities
Cladding	Zr	4.3365 -2*
Moderator	H	4.7769 -2
	O	2.3885 -2

* Read as 4.3365×10^{-2}

Along with comparison of multiplication factors (K_{inf}), the following effects were investigated:

- the Doppler effect for fuel temperature change from 660 to 960°C;
- the void effects for the coolant void fractures of 40, 70 and 95%.

For the comparison with the UNK and TRIFON calculational results, Japanese (the SWAT and SRAC95 codes) and German (the KAPROS/KARBUS and RESMOD/RSYST codes) results were chosen from [4]. The ITEP (Russian Federation) results were excluded because of enormous discrepancies. Japanese participants used nuclear cross-sections derived from the JENDL-3.2 data library. German nuclear data basically derived from the JEF-2.2 library with using the KEDAK4, ENDF/B-V and -VI libraries in the KAPROS calculations. The UNK and TRIFON calculations were performed using nuclear cross-sections based on ENDF/B-VI library.

All calculational results are summarized in Tables 1.13-1.15. The Doppler and void effects are given in units of pcm (10^{-5}). Besides, the mean values of interest together with standard deviations (σ) were calculated and summarized in Table 1.16. These values are very useful in investigation of discrepancies among the calculated results, because of comparison of the calculational data shows that there are significant disagreements, especially for the void effects at 95% void fraction.

Analysis of the data presented in Tables 1.13-1.16 shows that TRIFON overestimates the mean value of K_{inf} by up to 0.6% in cases with 0.0% MA content. But nevertheless, all K_{inf} values are within $\pm 2\sigma$, (from -400 to 670 pcm). The Doppler effect results are also agreed within $\pm 2\sigma$ ($\pm$45 pcm or $\pm$0.15 pcm/K).

The calculated data for the void effect are shown in Figures 1.1-1.3. Averaged values are fitted by curves for different MA contents and plotted with two standard deviations (2σ); the calculational data are represented as circles. Figures 1.1-1.3 indicate that the void effect becomes more positive with increase in the MA content. At the same time, the higher void fraction the higher discrepancy. As shown in Table 1.16 the largest discrepancies arise at 95% void fraction when the void effect is close to zero (cases MOX12 1.0% MA and MOX22 0.0% MA). Under these conditions an uncertainty in terms of 1σ (MOX22 0.0% MA) or 2σ (MOX12 1.0% MA) is larger than the mean value.

From the other hand, Table 1.16 reveals the fact that the values of standard deviations among all results are rather similar for the same effect. Summarizing deviations presented in Table 1.16 the following values for the mean deviations in K_{inf}, the Doppler and void effects can be derived (in terms of pcm):

- K_{inf} 290;
- the Doppler effect 26;
- the void effect at 40% void fraction 115;
- the void effect at 70% void fraction 221;
- the void effect at 95% void fraction 969.

Note that the void effect deviation is inversely proportional to the relative moderator density. It should be mentioned also that practically all the data on the void effect at 95% void fraction are within $\pm 1.7\sigma$. In other words, it means that the maximum uncertainty is about 3σ regardless the value of the effect. Therefore, there is no sense to analyze calculational uncertainties between different codes if it is expected that the value of the void effect be of order of $\pm 3\sigma$ ($\pm$3000 pcm in the current comparison).

Table 1.13. Comparison of Calculational Results for MOX12 Case (Standard Lattice)

MOX12 0.0% MA						
Parameter	SWAT	SRAC95	RESMOD	KAPROS	TRIFON	UNK
K_{inf}	1.10399	1.10854	1.1081	1.10694	1.11470	1.10854
Doppler	-990	-980	-	-1020	-948	-977
Void 40%	-8100	-8060	-8150	-8120	-8312	-8219
Void 70%	-13490	-13270	-13460	-13320	-13932	-13729
Void 95%	-15020	-12860	-14190	-14580	-12528	-14301

MOX12 1.0% MA						
Parameter	SWAT	SRAC95	RESMOD	KAPROS	TRIFON	UNK
K_{inf}	1.07879	1.08437	1.08080	1.08431	1.08345	1.08064
Doppler	-860	-860	-	-920	-901	-871
Void 40%	-5130	-5130	-5130	-4930	-5521	-5218
Void 70%	-5740	-5570	-5560	-5080	-5837	-5736
Void 95%	330	2610	1380	1800	3471	1683

MOX12 2.5% MA						
Parameter	SWAT	SRAC95	RESMOD	KAPROS	TRIFON	UNK
K_{inf}	1.06292	1.06956	1.06410	1.07079	1.06259	1.06438
Doppler	-760	-750	-	-830	-831	-791
Void 40%	-1790	-1840	-1720	-1510	-1966	-1775
Void 70%	1970	2090	2290	2840	2518	2372
Void 95%	14950	17330	16020	16910	18334	16700

Table 1.14. Comparison of Calculational Results for MOX22 Case (Standard Lattice)

MOX22 0.0% MA						
Parameter	SWAT	SRAC95	RESMOD	KAPROS	TRIFON	UNK
K_{inf}	1.12470	1.12957	1.12860	1.12585	1.13277	1.12598
Doppler	-940	-930	-	-1000	-961	-947
Void 40%	-5430	-5420	-5470	-5690	-5782	-5560
Void 70%	-6730	-6550	-6640	-6530	-6813	-6815
Void 95%	-2150	100	-1190	-1480	924	-851

MOX22 1.0% MA						
Parameter	SWAT	SRAC95	RESMOD	KAPROS	TRIFON	UNK
K_{inf}	1.10426	1.10968	1.10690	1.10371	1.10737	1.10427
Doppler	-850	-840	-	-910	-918	-868
Void 40%	-3460	-3480	-3470	-3380	-3714	-3524
Void 70%	-1860	-1700	-1670	-1480	-1591	-1681
Void 95%	7520	9880	8580	8550	10972	9208

MOX22 2.5% MA						
Parameter	SWAT	SRAC95	RESMOD	KAPROS	TRIFON	UNK
K_{inf}	1.08556	1.09186	1.08740	1.08391	1.08481	1.08605
Doppler	-750	-750	-	-820	-815	-794
Void 40%	-700	-750	-640	-560	-799	-622
Void 70%	4370	4500	4680	4920	5140	4952
Void 95%	19480	21930	20510	20830	22944	21402

Table 1.15. Comparison of Calculational Results for MOX22 Case
(Highly Moderated Lattice)

MOX22 0.0% MA wide						
Parameter	SWAT	SRAC95	RESMOD	KAPROS	TRIFON	UNK
K_{inf}	1.18209	1.18597	1.18680	1.18373	1.19298	1.18605
Doppler	-900	-890	-	-900	-891	-871
Void 40%	-10240	-10180	-10270	-10340	-10218	-10220
Void 70%	-21260	-21060	-21260	-21300	-21421	-21369
Void 95%	-27950	-25610	-27360	-27540	-26275	-27502

MOX22 1.0% MA wide						
Parameter	SWAT	SRAC95	RESMOD	KAPROS	TRIFON	UNK
K_{inf}	1.12559	1.13115	1.12860	1.12469	1.13407	1.12793
Doppler	-810	-800	-	-830	-825	-792
Void 40%	-9040	-9020	-9110	-9080	-9244	-9082
Void 70%	-16220	-16110	-16210	-16080	-16862	-16352
Void 95%	-14040	-11610	-13160	-13180	-12083	-13175

MOX22 2.5% MA wide						
Parameter	SWAT	SRAC95	RESMOD	KAPROS	TRIFON	UNK
K_{inf}	1.09050	1.09784	1.09290	1.08806	1.09433	1.09207
Doppler	-720	-710	-	-770	-788	-736
Void 40%	-6280	-6330	-6340	-6260	-6662	-6305
Void 70%	-7910	-7900	-7830	-7560	-8414	-7856
Void 95%	4080	6670	5050	5340	6656	5579

Table 1.16. Averaged Values (with One Standard Deviation)

Parameter	MOX12 0.0% MA	MOX12 1.0% MA	MOX12 2.5% MA
K_{inf}	1.10847 ± 0.00320	1.08206 ± 0.00211	1.06572 ± 0.00323
Doppler	-983 ± 23	-882 ± 24	-792 ± 34
Void 40%	-8160 ± 83	-5176 ± 177	-1767 ± 138
Void 70%	-13534 ± 231	-5587 ± 247	-2347 ± 284
Void 95%	-13913 ± 906	-1879 ± 980	-16707 ± 1052

Parameter	MOX22 0.0% MA	MOX22 1.0% MA	MOX22 2.5% MA
K_{inf}	1.12791 ± 0.00274	1.10603 ± 0.00214	1.08660 ± 0.00259
Doppler	-955 ± 24	-877 ± 32	-786 ± 31
Void 40%	-5559 ± 136	-3505 ± 103	-678 ± 80
Void 70%	-6680 ± 115	-1664 ± 115	4760 ± 269
Void 95%	-775 ± 1018	9118 ± 1095	21183 ± 1094

Parameter	MOX22 0.0% MA wide	MOX22 1.0% MA wide	MOX22 2.5% MA wide
K_{inf}	1.18627 ± 0.00340	1.12867 ± 0.00320	1.09262 ± 0.00305
Doppler	-890 ± 11	-811 ± 14	-745 ± 30
Void 40%	-10245 ± 50	-9096 ± 73	-6363 ± 136
Void 70%	-21278 ± 114	-16306 ± 264	-7912 ± 253
Void 95%	-27040 ± 819	-12875 ± 801	5563 ± 907

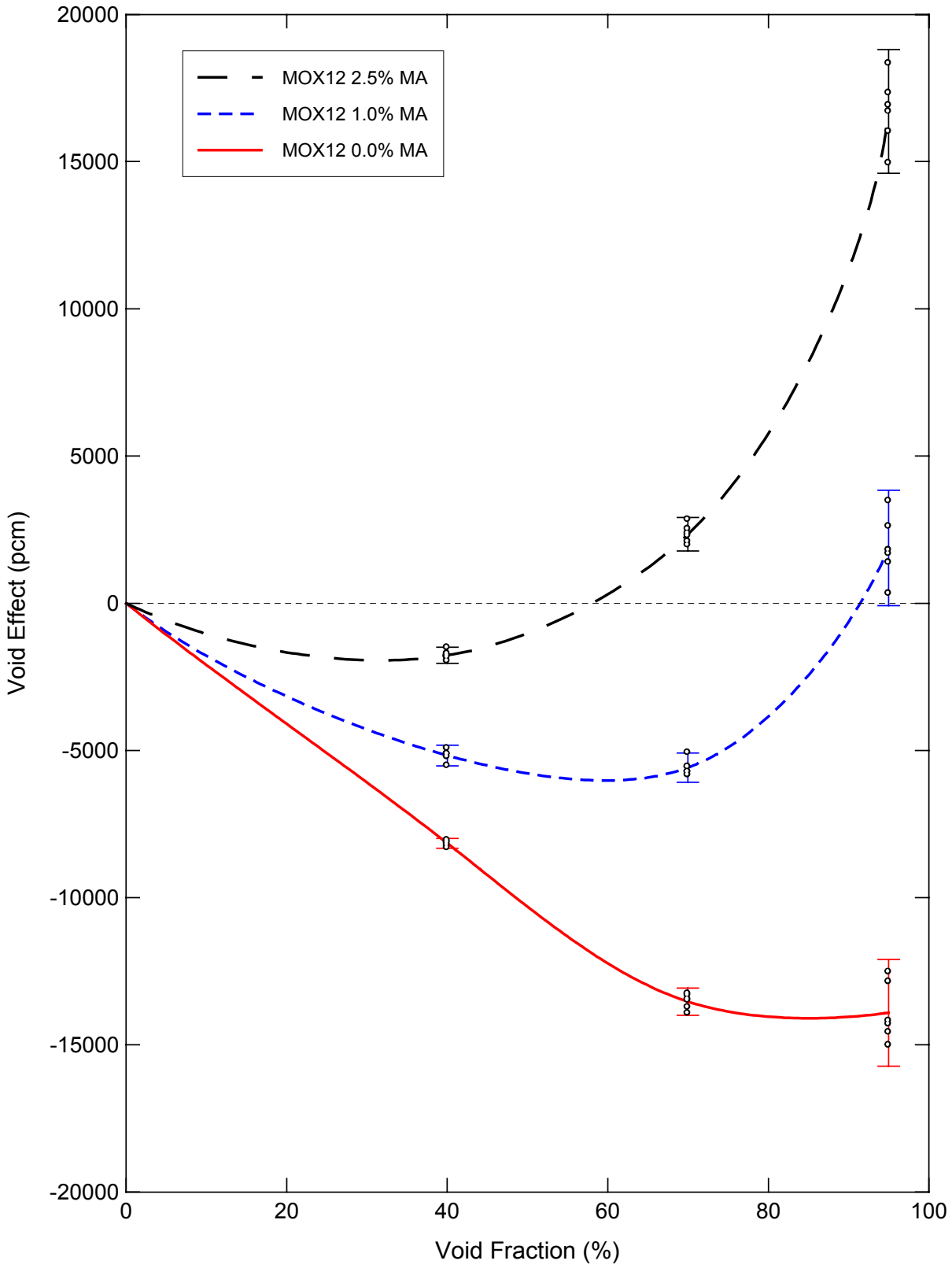

Figure 1.1. Void Effect for MOX12 Case (Standard Lattice) vs. Void Fraction

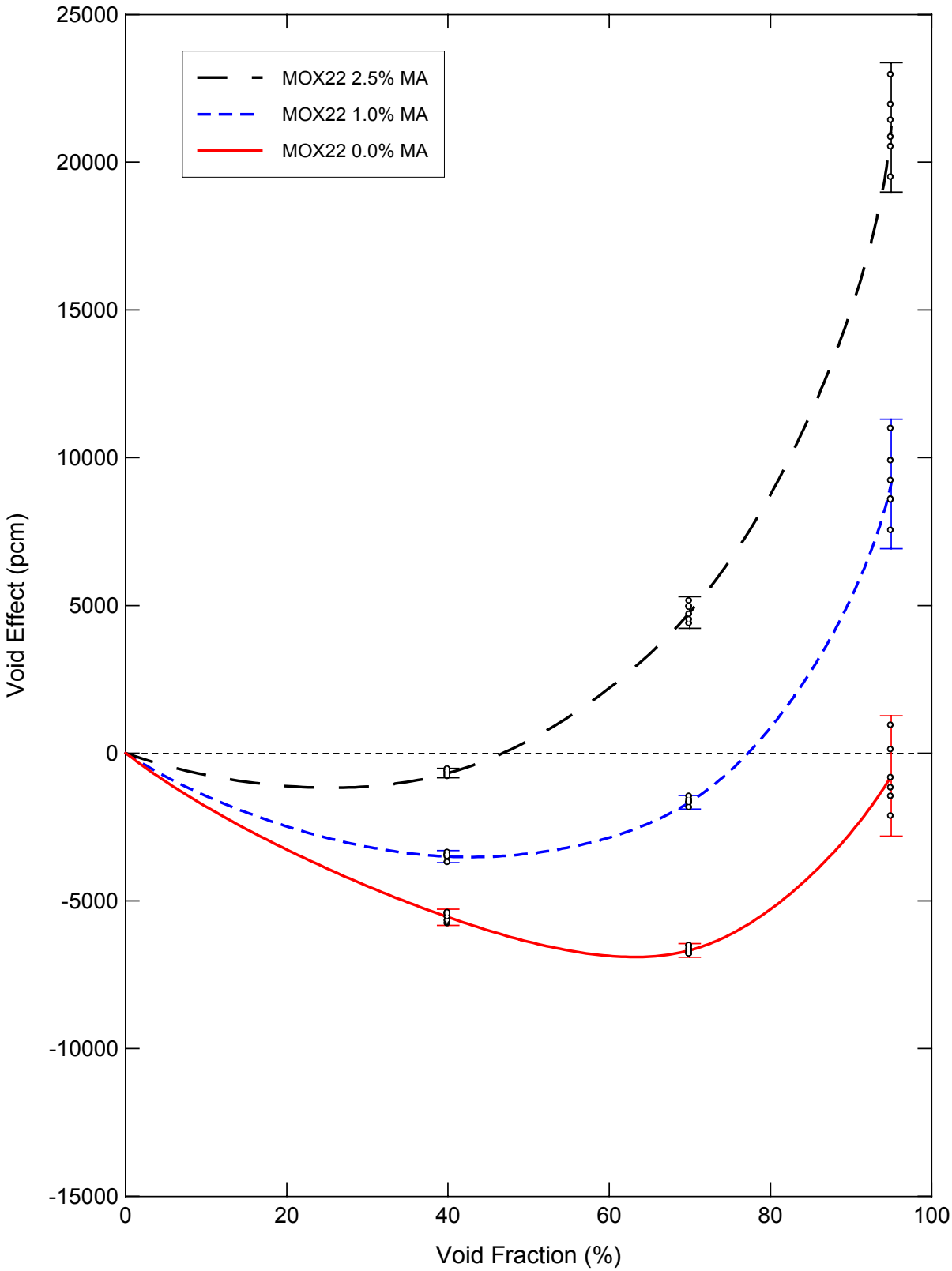

Figure 1.2. Void Effect for MOX22 Case (Standard Lattice) vs. Void Fraction

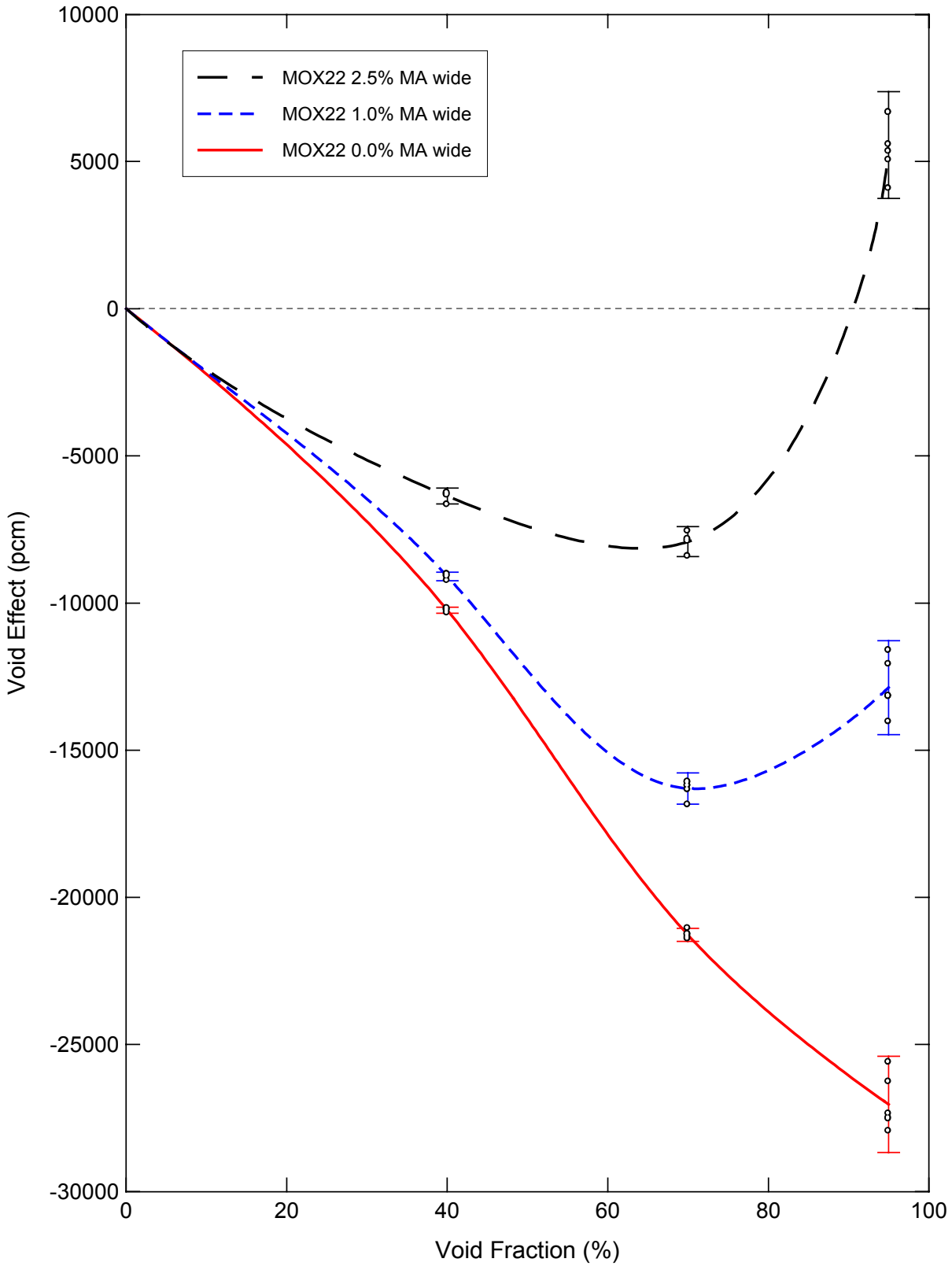

Figure 1.3. Void Effect for MOX22 Case (Highly Moderated Lattice) vs. Void Fraction

1.3 VVER Calculational Benchmark

This calculational benchmark represents typical VVER pin cell with 1.275-cm triangular lattice pitch [5]. The radii of the fuel, cladding and moderator are all the same for all variants and states: 0.386 and 0.4582 cm for fuel and cladding regions respectively. Equivalent outer cell radius is 0.669423 cm. Only zero-leakage cases were used for the current comparison. All cases are defined as combination of states (thermal-hydraulic parameters and presence or absence of absorbers in the fuel and moderator regions) and variants (fuel composition). The state parameters are given in Table 1.17. The calculational benchmarks are divided into variants, with five states in each of the variants. The variants differ only by fuel composition as shown in Table 1.18. The following types of fuel were investigated in the current comparison: fresh uranium fuel and fresh MOX fuel. There are five variations of the fresh MOX fuel: fresh MOX fuel, MOX fuel with ^{239}Pu only, MOX fuel with ^{240}Pu only, MOX fuel with ^{241}Pu only, and reactor-grade MOX fuel. Non-fuel material composition is presented in Table 1.19. There are three moderator material compositions. The variations in the moderator compositions are due to the presence or absence of boron, the cladding and moderator temperature, and the moderator density.

Table 1.17. State Parameters of Cells

State	Fuel region temperature (K)	Non-fuel region temperature (K)	^{135}Xe, ^{149}Sm in fuel	^{10}B, ^{11}B in moderator	Moderator material
S1	1027	579	Yes*	Yes	MOD1
S3	1027	579	Yes*	No	MOD2
S4	1027	579	No	Yes	MOD1
S5	579	579	No	Yes	MOD1
S6	300	300	No	Yes	MOD3

*Model of “equilibrium concentrations” (^{135}Xe: 9.4581×10^{-9}; ^{149}Sm: 7.3667×10^{-8})

The following effects of reactivity were investigated in the current intercomparison:

- the fuel temperature (Doppler) effect (states S5 – S4);
- the isothermal temperature effect (states S6 – S5);
- effect of presence of ^{135}Xe and ^{149}Sm in the fuel region (states S4 – S1)
- the boron poisoning effect (states S3 – S1).

Table 1.18. Fuel Material Composition for Variants

Variant	Comment	Nuclide	Number density (10^{-24} cm^{-3})
V1	Fresh uranium (UOX) fuel	^{235}U	8.7370 -4*
		^{238}U	1.8744 -2
		^{16}O	3.9235 -2
V2	Fresh MOX fuel	^{235}U	3.8393 -5
		^{238}U	1.8917 -2
		^{239}Pu	6.5875 -4
		^{240}Pu	4.2323 -5
		^{241}Pu	7.0246 -4
		^{16}O	4.1707 -2
V7	Fresh MOX fuel with ^{239}Pu only	^{235}U	3.8393 -5
		^{238}U	1.8917 -2
		^{239}Pu	6.5875 -4
		^{16}O	4.1707 -2
V8	Fresh MOX fuel with ^{240}Pu only	^{235}U	6.9714 -4
		^{238}U	1.8917 -2
		^{240}Pu	4.2323 -4
		^{16}O	4.1707 -2
V9	Fresh MOX fuel with ^{241}Pu only	^{235}U	3.8393 -5
		^{238}U	1.8917 -2
		^{241}Pu	6.6577 -4
		^{16}O	4.1707 -2
V10	Fresh MOX fuel (reactor-grade)	^{235}U	5.0000 -5
		^{238}U	2.2100 -2
		^{238}Pu	3.0000 -5
		^{239}Pu	1.1600 -3
		^{240}Pu	4.9000 -4
		^{241}Pu	1.9000 -4
		^{242}Pu	1.0500 -4
		^{241}Am	2.5000 -5
		^{16}O	4.6300 -2

*Read as 8.7370×10^{-4}

Table 1.19. Non-fuel Material Composition

Material	Comment	Nuclide	Number density (10^{-24} cm^{-3})
Clad	Cladding	Zr	4.2300 -2*
MOD1	Hot moderator with boric acid	H	4.7830 -2
		^{16}O	2.3910 -2
		^{10}B	4.7344 -6
		^{11}B	1.9177 -5
MOD2	Hot moderator without boric acid	H	4.7830 -2
		^{16}O	2.3910 -2
MOD3	Cold moderator with boric acid	H	6.6940 -2
		^{16}O	3.3470 -2
		^{10}B	6.6262 -6
		^{11}B	2.6839 -5

*Read as 4.2300×10^{-2}

Calculational results presented in [5] were performed using the MCU-RFFI/A Monte Carlo code with the MCUDAT library. Statistical error in calculations of multiplication factor (K_{inf}) was estimated as less than 0.1%. Four-group neutron balances for cases V1S1 and V2S1 are also presented there. Results presented in [6] were obtained using SCALE-4.3/SAS2H and compared with the data calculated by different codes including HELIOS-1.4 [7]. The same calculations were performed using the SCALE5.0 code with two different sequences for processing cross-section data labeled as NITAWL (a standard option) and CENTRM [8]. All the SCALE results were calculated with nuclear cross-sections based on ENDF/B-V. HELIOS as well as UNK and TRIFON used nuclear cross-sections based on ENDF/B-VI.

The results obtained by HELIOS, MCU-RFFI/A (only for variants V1 and V2), UNK, TRIFON and three versions of SCALE are summarized in Tables 1.20-1.31. Reactivity effects were determined as differences between K_{inf} for the corresponding cases and given in units of pcm (10^{-5}). The mean values are shown with one standard deviation (σ). Deviations of the calculated effects from the mean values are given in brackets.

Because practically in all cases the SCALE calculations showed extremely different K_{inf} values compared with the rest, their results were not taken into account to calculate the mean values and shown separately below each table.

Comparison of neutron balances calculated by four codes for cases V1S1 (UOX) and V2S1 (MOX) is shown in Tables 1.32 and 1.33 (with total neutron absorption normalized to 10^5).

Table 1.20. Comparison of K_{inf} Calculational Results for UOX Cell V1

	Case V1S1	Case V1S3	Case V1S4	Case V1S5	Case V1S6
HELIOS-1.4	1.2750	1.3315	1.3227	1.3393	1.3754
MCU-RFFI/A	1.2743	-	1.3219	1.3382	1.3739
TRIFON	1.27101	1.32739	1.31899	1.33629	1.37372
UNK	1.27472	1.33110	1.32291	1.33951	1.37653
Mean value	1.27376 ± 0.00160	1.33000 ± 0.00185	1.32162 ± 0.00157	1.33832 ± 0.00128	1.37489 ± 0.00115
SCALE/SAS2H	1.2589	1.3140	1.3065	1.3245	1.3669
SCALE/NITAWL	1.2593	1.3144	1.3069	1.3249	1.3669
SCALE/CENTRM	1.2541	1.3090	1.3015	1.3205	1.3634

Table 1.21. Comparison for Reactivity Effects (pcm) in UOX Cell V1

	Doppler Cases S5 – S4	Isothermal Cases S6 – S5	^{135}Xe, ^{149}Sm Cases S4 – S1	Boron Cases S3 – S1
HELIOS-1.4	1660 (-10)	3610 (-46)	4770 (-17)	5650 (8)
MCU-RFFI/A	1630 (-40)	3570 (-86)	4760 (-27)	-
TRIFON	1730 (60)	3743 (87)	4798 (11)	5637 (-5)
UNK	1660 (-10)	3702 (46)	4819 (32)	5638 (-4)
Mean value	1670 ± 37	3656 ± 69	4787 ± 23	5642 ± 6
SCALE/SAS2H	1800 (130)	4240 (584)	4760 (-27)	5510 (-132)
SCALE/NITAWL	1800 (130)	4200 (544)	4760 (-27)	5510 (-132)
SCALE/CENTRM	1900 (230)	4290 (634)	4740 (-47)	5490 (-152)

Note: In brackets – deviations from the mean values calculated excluding the SCALE data.

Table 1.22. Comparison of K_{inf} Calculational Results for MOX Cell V2

	Case V2S1	Case V2S3	Case V2S4	Case V2S5	Case V2S6
HELIOS-1.4	1.2188	1.2481	1.2383	1.2583	1.3309
MCU-RFFI/A	1.2135	-	1.2331	1.2514	1.3242
TRIFON	1.21567	1.24582	1.23614	1.25621	1.32811
UNK	1.21165	1.24072	1.23139	1.25096	1.32430
Mean value	1.21490 ± 0.00266	1.24488 ± 0.00309	1.23473 ± 0.00267	1.25422 ± 0.00313	1.32688 ± 0.00281
SCALE/SAS2H	1.2054	1.2339	1.2250	1.2466	1.3248
SCALE/NITAWL	1.2074	1.2360	1.2270	1.2474	1.3256
SCALE/CENTRM	1.2017	1.2300	1.2212	1.2428	1.3210

Table 1.23. Comparison for Reactivity Effects (pcm) in MOX Cell V2

	Doppler Cases S5 – S4	Isothermal Cases S6 – S5	^{135}Xe, ^{149}Sm Cases S4 – S1	Boron Cases S3 – S1
HELIOS-1.4	2000 (51)	7260 (-6)	1950 (-33)	2930 (-21)
MCU-RFFI/A	1830 (-119)	7280 (14)	1960 (-23)	-
TRIFON	2007 (59)	7191 (-76)	2047 (64)	3016 (65)
UNK	1957 (9)	7334 (68)	1973 (-9)	2906 (-44)
Mean value	1949 ± 71	7266 ± 51	1983 ± 38	2951 ± 47
SCALE/SAS2H	2160 (210)	7820 (554)	1960 (-23)	2850 (-101)
SCALE/NITAWL	2040 (91)	7820 (554)	1960 (-23)	2860 (-91)
SCALE/CENTRM	2160 (210)	7820 (554)	1950 (-33)	2830 (-121)

Note: In brackets – deviations from the mean values calculated excluding the SCALE data.

Table 1.24. Comparison of K_{inf} Calculational Results for MOX Cell V7

	Case V7S1	Case V7S3	Case V7S4	Case V7S5	Case V7S6
HELIOS-1.4	1.3189	1.3523	1.3412	1.3584	1.4181
TRIFON	1.31011	1.34405	1.33323	1.35108	1.41065
UNK	1.31089	1.34402	1.33334	1.35032	1.41022
Mean value	1.31330 ± 0.00397	1.34679 ± 0.00390	1.33593 ± 0.00373	1.35327 ± 0.00364	1.41299 ± 0.00362
SCALE/SAS2H	1.3036	1.3361	1.3259	1.3445	1.4105
SCALE/NITAWL	1.3047	1.3372	1.3270	1.3459	1.4112
SCALE/CENTRM	1.2984	1.3307	1.3206	1.3404	1.4067

Table 1.25. Comparison for Reactivity Effects (pcm) in MOX Cell V7

	Doppler Cases S5 – S4	Isothermal Cases S6 – S5	^{135}Xe, ^{149}Sm Cases S4 – S1	Boron Cases S3 – S1
HELIOS-1.4	1720 (-14)	5970 (-20)	2230 (-32)	3340 (-9)
TRIFON	1785 (51)	5957 (-15)	2312 (49)	3394 (45)
UNK	1698 (-36)	5990 (1)	2245 (-17)	3313 (-36)
Mean value	1734 ± 37	5972 ± 14	2262 ± 35	3349 ± 34
SCALE/SAS2H	1860 (126)	6600 (628)	2230 (-32)	3250 (-99)
SCALE/NITAWL	1890 (156)	6530 (558)	2230 (-32)	3250 (-99)
SCALE/CENTRM	1980 (246)	6630 (658)	2220 (-42)	3230 (-119)

Note: In brackets – deviations from the mean values calculated excluding the SCALE data.

Table 1.26. Comparison of K_{inf} Calculational Results for MOX Cell V8

	Case V8S1	Case V8S3	Case V8S4	Case V8S5	Case V8S6
HELIOS-1.4	1.1044	1.1595	1.1540	1.1728	1.2191
TRIFON	1.10865	1.16410	1.15877	1.17775	1.22377
UNK	1.10454	1.15958	1.15459	1.17326	1.22093
Mean value	1.10586 ± 0.00197	1.16106 ± 0.00215	1.15579 ± 0.00212	1.17460 ± 0.00224	1.22127 ± 0.00192
SCALE/SAS2H	1.0896	1.1434	1.1390	1.1593	1.2115
SCALE/NITAWL	1.0904	1.1442	1.1399	1.1596	1.2115
SCALE/CENTRM	1.0859	1.1395	1.1351	1.1557	1.2084

Table 1.27. Comparison for Reactivity Effects (pcm) in MOX Cell V8

	Doppler Cases S5 – S4	Isothermal Cases S6 – S5	^{135}Xe, ^{149}Sm Cases S4 – S1	Boron Cases S3 – S1
HELIOS-1.4	1880 (-2)	4630 (-36)	4960 (-33)	5510 (-10)
TRIFON	1899 (17)	4602 (-65)	5012 (20)	5545 (25)
UNK	1867 (-15)	4768 (102)	5005 (13)	5504 (-16)
Mean value	1882 ± 13	4666 ± 73	4992 ± 23	5520 ± 18
SCALE/SAS2H	2030 (148)	5220 (554)	4940 (-53)	5380 (-140)
SCALE/NITAWL	1970 (88)	5190 (524)	4950 (-43)	5380 (-140)
SCALE/CENTRM	2060 (178)	5270 (604)	4920 (-73)	5360 (-160)

Note: In brackets – deviations from the mean values calculated excluding the SCALE data.

Table 1.28. Comparison of K_{inf} Calculational Results for MOX Cell V9

	Case V9S1	Case V9S3	Case V9S4	Case V9S5	Case V9S6
HELIOS-1.4	1.5722	1.6103	1.5960	1.6166	1.6508
TRIFON	1.56753	1.60592	1.59193	1.61268	1.64614
UNK	1.56839	1.60565	1.59208	1.61170	1.64859
Mean value	1.56937 ± 0.00203	1.60729 ± 0.00213	1.59334 ± 0.00188	1.61363 ± 0.00207	1.64851 ± 0.00190
SCALE/SAS2H	1.5279	1.5633	1.5503	1.5732	1.6189
SCALE/NITAWL	1.5290	1.5644	1.5515	1.5736	1.6195
SCALE/CENTRM	1.5207	1.5561	1.5432	1.5668	1.6140

Table 1.29. Comparison for Reactivity Effects (pcm) in MOX Cell V9

	Doppler Cases S5 – S4	Isothermal Cases S6 – S5	^{135}Xe, ^{149}Sm Cases S4 – S1	Boron Cases S3 – S1
HELIOS-1.4	2050 (21)	3430 (-60)	2380 (-16)	3810 (19)
TRIFON	2076 (46)	3346 (-142)	2439 (43)	3838 (47)
UNK	1962 (-67)	3688 (198)	2369 (-27)	3726 (-65)
Mean value	2029 ± 49	3488 ± 146	2396 ± 31	3792 ± 48
SCALE/SAS2H	2290 (261)	4570 (1082)	2240 (-156)	3540 (-252)
SCALE/NITAWL	2210 (181)	4590 (1102)	2250 (-146)	3540 (-252)
SCALE/CENTRM	2360 (331)	4720 (1232)	2250 (-146)	3540 (-252)

Note: In brackets – deviations from the mean values calculated excluding the SCALE data.

Table 1.30. Comparison of K_{inf} Calculational Results for MOX Cell V10

	Case V10S1	Case V10S3	Case V10S4	Case V10S5	Case V10S6
HELIOS-1.4	1.1136	1.1270	1.1195	1.1381	1.2091
TRIFON	1.11016	1.12401	1.11637	1.13475	1.20721
UNK	1.10226	1.11547	1.10819	1.12568	1.19752
Mean value	1.10867 ± 0.00475	1.12216 ± 0.00489	1.11469 ± 0.00477	1.13284 ± 0.00525	1.20461 ± 0.00507
SCALE/SAS2H	1.0950	1.1076	1.1007	1.1194	1.1937
SCALE/NITAWL	1.0952	1.1078	1.1010	1.1196	1.1937
SCALE/CENTRM	1.0902	1.1027	1.0958	1.1160	1.1917

Table 1.31. Comparison for Reactivity Effects (pcm) in MOX Cell V10

	Doppler Cases S5 – S4	Isothermal Cases S6 – S5	^{135}Xe, ^{149}Sm Cases S4 – S1	Boron Cases S3 – S1
HELIOS-1.4	1860 (44)	7100 (-77)	590 (-12)	1340 (-9)
TRIFON	1838 (22)	7246 (69)	621 (20)	1385 (36)
UNK	1749 (-67)	7184 (8)	594 (-8)	1322 (-27)
Mean value	1816 ± 48	7177 ± 60	602 ± 14	1349 ± 27
SCALE/SAS2H	1870 (54)	7430 (253)	570 (-32)	1260 (-89)
SCALE/NITAWL	1860 (64)	7410 (233)	580 (-22)	1260 (-89)
SCALE/CENTRM	2020 (204)	7570 (393)	560 (-42)	1250 (-99)

Note: In brackets – deviations from the mean values calculated excluding the SCALE data.

Table 1.32. Neutron Balance Comparison for UOX Case V1S1

		MCU-RFFI/A	TRIFON	UNK	HELIOS
^{235}U	Fission	48 587	48 760	48 837	-
	Capture	11 244	11 431	11 343	-
	Absorption	59 831	60 192	60 180	60 190
^{238}U	Fission	3 090	2 960	2 973	-
	Capture	26 548	26 361	26 314	-
	Absorption	29 638	29 321	29 286	29 170
Xe+Sm	Capture	2 739	2 762	2 769	2 704
Zr	Capture	1 109	1 027	1 064	-
^{10}B	Capture	3 329	3 344	3 339	-
H+O	Capture	3 349	3 356	3 361	-

Table 1.33. Neutron Balance Comparison for MOX Case V2S1

		MCU-RFFI/A	TRIFON	UNK	HELIOS
^{235}U	Fission	1 133	1 160	1 117	-
	Capture	322	344	328	-
	Absorption	1 455	1 504	1 444	1 462
^{238}U	Fission	3 197	2 975	3 117	-
	Capture	24 221	24 304	23 974	-
	Absorption	27 418	27 278	27 091	26 940
^{239}Pu	Fission	37 585	37 975	37 703	-
	Capture	20 775	20 733	20 889	-
	Absorption	58 360	58 708	58 592	58 520
^{240}Pu	Fission	40	38	38	-
	Capture	6 125	5 873	6 316	-
	Absorption	6 165	5 910	6 354	6 365
^{241}Pu	Fission	476	498	485	-
	Capture	176	160	156	-
	Absorption	651	659	641	640
Xe+Sm	Capture	1 147	1 181	1 141	1 113
Zr	Capture	941	867	899	-
^{10}B	Capture	1 799	1 841	1 783	-
H+O	Capture	2 063	2 051	2 055	-

For the UOX fuel as shown in Tables 1.20 and 1.21, HELIOS, MCU, TRIFON and UNK calculate the multiplication factor with high accuracy: the maximum difference in the K_{inf} value is about 0.3%. Reactivity effects are also in good agreement (with the maximum deviation of 6% in the Doppler effect). The K_{inf} values calculated by all the SCALE versions are lower by 0.6–1.6% and the Doppler and isothermal effects are highly different (by 8–17%) from the mean values obtained by previous codes. These large differences in K_{inf} and the reactivity effects (shown in brackets) are probably due to using different data libraries (ENDF/B-VI vs. ENDF/B-V) to generate cross-sections.

For the MOX fuel cell V2 (see Tables 1.22 and 1.23), the maximum differences in K_{inf} and the Doppler effect are 0.5–0.6% and 9% respectively (for HELIOS, MCU, TRIFON and UNK). SCALE/NITAWL gives slightly lower K_{inf} results (about -0.6%), but except for the case V2S6, the SCALE/SAS2H and SCALE/CENTRM calculations have lower K_{inf} values (from -0.6 to -1.2%). As in the UOX fuel cases, the same trends are observed for the reactivity effects: overestimation of the Doppler and isothermal effects.

The MOX fuel cell V7 differs from the previous cell only by absent of ^{240}Pu and ^{241}Pu in the fuel region. ^{239}Pu absorption rate reaches about 70% in the neutron balance. As in the MOX fuel cell V2, the HELIOS code gives slightly larger K_{inf} values (see Tables 1.24 and 1.25) and all previous conclusions about K_{inf} and the reactivity effects are valid too.

The MOX fuel cell V8 represents, in general, fresh UOX fuel with addition of ^{240}Pu whose absorption rate is only about 7% in the neutron balance. For this reason differences in K_{inf} and the reactivity effects (see Tables 1.26 and 1.27) are close to those for the UOX fuel.

The MOX fuel cell V9 contains the only nuclide of Pu – ^{241}Pu, whose absorption rate is about 70% in the neutron balance. The maximum difference in the reactivity effects (in the isothermal effect) between HELIOS, TRIFON and UNK reaches about 10%. The SCALE versions, as shown in Tables 1.28 and 1.29, significantly underestimate the K_{inf} values (by 2–3%); the deviations in the isothermal effect reach more than 30% in comparison with the HELIOS, TRIFON and UNK results.

At last, the MOX fuel cell V10 represents a fresh MOX fuel containing recycled reactor Pu. For this variant the differences between the HELIOS and UNK multiplication factors K_{inf} reaches about 1% as shown in Tables 1.30 and 1.31. The maximum difference in reactivity effects is about 6% (the Doppler effect). The SCALE results for K_{inf} are 0.9–1.7% lower but nevertheless, the reactivity effects are predicted with rather good accuracy (except for the SCALE/CENTRM results).

Comparisons of the neutron balance for cases V1S1 and V2S1 (see Tables 1.32 and 1.33) show that the reaction rates for major important nuclides are in very good agreement for the UOX fuel (V1S1). For the MOX fuel (V2S1) presented reaction rates are also well agreed. It should be mentioned an excellent agreement between the UNK and HELIOS results.

1.4. Benchmark Calculations of Power Distribution within Fuel Assemblies

This benchmark model has been proposed to compare different approaches of diffusion and transport methods as well as nuclear data sets. Detailed specification of the benchmark is given in [9]. Here only the pin cell models are considered. There are four types of cells: one UOX cell with ^{235}U enrichment of 3.7% and three MOX cells with different plutonium enrichments (4.3%, 7.0% and 8.7%). The temperature is assumed to be constant and equal to 20°C.

The nuclide number densities for different cases are presented in Tables 1.34 and 1.35. Each cell contains the fuel region, two cladding regions made of Zr and Al respectively, and the moderator region as well as two void gaps inside each cladding. The fuel and cladding radii are 0.4095, 0.475 and 0.54 cm respectively; outer cell radius is 0.710879 cm (1.26-cm square lattice pitch). Zr cladding thickness is 0.57 mm and Al cladding thickness - 0.55 mm.

Table 1.34. Fuel Number Densities (10^{-24} cm^{-3})

Nuclide	UOX fuel	MOX 4.3%	MOX 7.0%	MOX 8.7%
^{235}U	8.650 -4*	5.00 -5	5.00 -5	5.00 -5
^{238}U	2.225 -2	2.21 -2	2.21 -2	2.21 -2
^{238}Pu	-	1.50 -5	2.40 -5	3.00 -5
^{239}Pu	-	5.80 -4	9.30 -4	1.16 -3
^{240}Pu	-	2.40 -4	3.90 -4	4.90 -4
^{241}Pu	-	9.80 -5	1.52 -4	1.90 -4
^{242}Pu	-	5.40 -5	8.40 -5	1.05 -4
^{241}Am	-	1.30 -5	2.00 -5	2.50 -5
O	4.662 -2	4.63 -2	4.63 -2	4.63 -2

* Read as 8.650×10^{-4}

Table 1.35. Cladding and Moderator Number Densities (10^{-24} cm^{-3})

Region	Material	Number Density
Zr Cladding	Zr nat.	4.30 -2*
Al Cladding	^{27}Al	6.00 -2
Moderator	H_2O	3.35 -2
	B nat.	2.78 -5

* Read as 4.30×10^{-2}

In the current comparison with the UNK and TRIFON calculations, 11 sets of calculational data presented in [9] were used. Among them the only one continuos-energy Monte Carlo code applied was MVP (JAERI). All participants used different nuclear cross-sections data derived from different libraries (widely spread JEF-2.2, ENDF/B-VI, JENDL-3.2 and FOND-2.2, as well as, the older versions: JEF-1 and MOL-BR2-40GR). The TRIFON and UNK calculations were performed using nuclear cross-sections based on ENDF/B-VI.

Calculational results for multiplication factors are summarized in Table 1.36. At the bottom of the table there are the mean values of K_{inf} with one standard deviation (σ). Deviations of the calculated data from the mean value are included in Table 1.37 in terms of pcm (10^{-5}) and in percents in brackets. Comparisons of neutron balances calculated by different codes for UOX and MOX cells are shown in Tables 1.38-1.41 (with total neutron absorption normalized to 10^5). Data obtained by UNK and TRIFON are compared with those for some selected codes: APOLLO-2 (CEA), WIMS7A, HELIOS and SRAC95. Note that original HELIOS data presented in [9] indicate overestimated total absorption rate; for the current intercomparison they were properly re-normalized taking into account the contribution of Al and Zr to the total absorption.

Table 1.36. Comparison of K_{inf} Calculational Results

	UOX fuel	MOX 4.3%	MOX 7.0%	MOX 8.7%
APOLLO-2 (CEA)	1.32707	1.13710	1.16188	1.17558
APOLLO-2 (EDF)	1.32735	1.13723	1.16170	1.17524
RESMOD	1.32100	1.13000	1.15500	1.16900
WIMS7A	1.32213	1.13196	1.15749	1.17185
SCALE-4.2	1.31720	1.13290	1.15940	1.17430
BOXER	1.31420	1.13900	1.16510	1.17920
HELIOS	1.32651	1.12853	1.15421	1.16908
WIMSD-4	1.31643	1.13299	1.15931	1.17411
SRAC95	1.32303	1.14152	1.16879	1.18373
MVP	1.33200	1.13990	1.16470	1.17860
MULCOS	1.33146	1.18046*	1.20245*	1.21441*
TRIFON	1.32698	1.14067	1.16637	1.17923
UNK	1.32755	1.13295	1.15633	1.16936
Mean value	1.32407 ± 0.00541	1.13540 ± 0.00419	1.16086 ± 0.00450	1.17494 ± 0.00446

**These data were not taken into account to calculate the mean values*

Table 1.37. Deviations of K_{inf} (pcm) from the Mean Values

	UOX fuel	MOX 4.3%	MOX 7.0%	MOX 8.7%
APOLLO-2 (CEA)	300 (0.2)	170 (0.1)	102 (0.1)	64 (0.1)
APOLLO-2 (EDF)	328 (0.2)	183 (0.2)	84 (0.1)	30 (0.0)
RESMOD	-307 (-0.2)	-540 (-0.5)	-586 (-0.5)	-594 (-0.5)
WIMS7A	-194 (-0.2)	-344 (-0.3)	-337 (-0.3)	-309 (-0.3)
SCALE-4.2	-687 (-0.5)	-250 (-0.2)	-146 (-0.1)	-64 (-0.1)
BOXER	-987 (-0.7)	360 (0.3)	424 (0.4)	426 (0.4)
HELIOS	244 (0.2)	-687 (-0.6)	-665 (-0.6)	-586 (-0.5)
WIMSD-4	-764 (-0.6)	-241 (-0.2)	-155 (-0.1)	-83 (-0.1)
SRAC95	-104 (-0.1)	612 (0.5)	793 (0.7)	879 (0.8)
MVP	793 (0.6)	450 (0.4)	384 (0.3)	366 (0.3)
MULCOS	739 (0.6)	4506 (4.0)	4159 (3.6)	3947 (3.4)
TRIFON	291 (0.2)	528 (0.5)	551 (0.5)	429 (0.4)
UNK	348 (0.3)	-245 (-0.2)	-453 (-0.4)	-558 (-0.5)

**In brackets – deviations in percents*

Table 1.38. Neutron Balance Comparison for UOX Fuel

		APOLLO	WIMS7A	HELIOS*	SRAC95	TRIFON	UNK
^{235}U	Fission	50 400	50 320	50 293	51 170	50 890	50 884
	Capture	11 130	11 030	11 514	11 080	11 360	11 324
	Absorption	61 530	61 350	61 807	62 250	62 250	62 208
^{238}U	Fission	3 428	3 392	3 318	2 961	3 076	3 089
	Capture	26 472	26 608	26 376	25 879	25 916	25 925
	Absorption	29 900	30 000	29 694	28 840	28 993	29 014
B	Capture	3 298	3 317	3 253	3 470	3 380	3 376
H+O	Capture	3 959	3 977	3 895	3 911	3 986	3 994

**Re-normalized data*

Table 1.39. Neutron Balance Comparison for MOX 4.3%

		APOLLO	WIMS7A	HELIOS*	SRAC95	TRIFON	UNK
^{235}U	Fission	1 397	1 400	1 388	1 427	1 463	1 399
	Capture	386	385	411	387	419	398
	Absorption	1 783	1 785	1 800	1 814	1 882	1 797
^{238}U	Fission	3 278	3 167	3 222	3 113	3 051	3 169
	Capture	22 252	22 393	22 116	21 927	22 271	22 091
	Absorption	25 530	25 560	25 338	25 040	25 322	25 261
^{238}Pu	Fission	41	41	39	40	38	38
	Capture	299	302	307	305	325	312
	Absorption	340	343	346	345	363	350
^{239}Pu	Fission	28 620	28 600	28 535	28 990	28 895	28 683
	Capture	15 080	15 030	14 966	15 100	14 892	15 107
	Absorption	43 700	43 630	43 502	44 090	43 787	43 790
^{240}Pu	Fission	205	203	196	185	184	188
	Capture	13 305	13 217	13 816	13 355	12 933	13 294
	Absorption	13 510	13 420	14 012	13 540	13 117	13 482
^{241}Pu	Fission	6 052	6 068	6 026	5 989	6 215	6 050
	Capture	1 974	1 986	1 939	2 018	2 001	1 952
	Absorption	8 026	8 054	7 965	8 007	8 216	8 002
^{242}Pu	Fission	35	34	33	32	32	33
	Capture	1 321	1 377	1 324	1 278	1 360	1 460
	Absorption	1 356	1 411	1 358	1 310	1 392	1 493
^{241}Am	Fission	15	15	15	14	15	15
	Capture	964	960	930	883	957	926
	Absorption	979	975	945	897	972	941
B	Capture	1 643	1 665	1 595	1 750	1 731	1 672
H+O	Capture	2 228	2 213	2 165	2 132	2 246	2 236

**Re-normalized data*

Table 1.40. Neutron Balance Comparison for MOX 7.0%

		APOLLO	WIMS7A	HELIOS*	SRAC95	TRIFON	UNK
^{235}U	Fission	960	963	956	982	1 008	959
	Capture	301	300	325	302	331	313
	Absorption	1 261	1 263	1 281	1 284	1 338	1 272
^{238}U	Fission	3 274	3 162	3 223	3 093	3 026	3 145
	Capture	20 446	20 568	20 328	20 097	20 456	20 322
	Absorption	23 720	23 730	23 551	23 190	23 482	23 467
^{238}Pu	Fission	59	59	57	57	55	55
	Capture	308	312	319	316	333	321
	Absorption	367	371	376	373	388	376
^{239}Pu	Fission	29 320	29 300	29 222	29 790	29 708	29 376
	Capture	15 660	15 590	15 490	15 650	15 513	15 708
	Absorption	44 980	44 890	44 712	45 440	45 221	45 084
^{240}Pu	Fission	330	326	316	297	295	300
	Capture	14 520	14 414	15 105	14 603	14 172	14 477
	Absorption	14 850	14 740	15 421	14 900	14 467	14 777
^{241}Pu	Fission	6 364	6 414	6 364	6 296	6 494	6 347
	Capture	2 022	2 056	1 981	2 072	2 008	1 979
	Absorption	8 386	8 470	8 345	8 368	8 501	8 326
^{242}Pu	Fission	54	53	52	49	49	50
	Capture	1 596	1 674	1 547	1 545	1 625	1 811
	Absorption	1 650	1 727	1 599	1 594	1 675	1 861
^{241}Am	Fission	21	21	21	19	20	20
	Capture	1 089	1 086	1 050	994	1 111	1 047
	Absorption	1 110	1 107	1 071	1 013	1 131	1 067
B	Capture	1 167	1 190	1 126	1 259	1 237	1 259
H+O	Capture	1 727	1 711	1 671	1 613	1 722	1 728

**Re-normalized data*

Table 1.41. Neutron Balance Comparison for MOX 8.7%

		APOLLO	WIMS7A	HELIOS*	SRAC95	TRIFON	UNK
^{235}U	Fission	813	816	804	832	856	812
	Capture	270	269	291	271	299	283
	Absorption	1 083	1 085	1 095	1 103	1 155	1 095
^{238}U	Fission	3 269	3 157	3 189	3 079	3 010	3 128
	Capture	19 621	19 723	19 321	19 271	19 661	19 525
	Absorption	22 890	22 880	22 510	22 350	22 671	22 653
^{238}Pu	Fission	71	71	69	69	66	65
	Capture	316	320	326	323	341	329
	Absorption	387	391	395	392	407	394
^{239}Pu	Fission	29 480	29 460	29 102	29 990	29 870	29 547
	Capture	15 790	15 690	16 407	15 780	15 602	15 862
	Absorption	45 270	45 150	45 510	45 770	45 473	45 409
^{240}Pu	Fission	412	407	392	370	368	374
	Capture	14 938	14 813	15 379	15 050	14 657	14 887
	Absorption	15 350	15 220	15 771	15 420	15 025	15 261
^{241}Pu	Fission	6 659	6 735	6 616	6 584	6 781	6 624
	Capture	2 083	2 133	2 018	2 144	2 046	2 021
	Absorption	8 742	8 868	8 634	8 728	8 827	8 645
^{242}Pu	Fission	67	66	65	61	61	63
	Capture	1 728	1 817	1 641	1 674	1 755	1 955
	Absorption	1 795	1 883	1 705	1 735	1 817	2 018
^{241}Am	Fission	25	25	24	23	24	24
	Capture	1 169	1 166	1 118	1 067	1 209	1 126
	Absorption	1 194	1 191	1 142	1 090	1 233	1 150
B	Capture	1 001	1 023	954	1 086	1 065	1 026
H+O	Capture	1 550	1 535	1 484	1 428	1 538	1 550

**Re-normalized data*

Analysis of the data presented in Tables 1.36 and 1.37 shows that in case of the UOX fuel, a large spread of the K_{inf} values is observed; the maximum deviation reaches 1780 pcm or 1.3% between the MVP and BOXER results. This is larger than usually expected for the UOX fuel. It will be noted that the BOXER code used cross sections obtained from out-of-date nuclear data library JEF-1. As seen from Table 1.38, all selected codes (APOLLO-2, WIMS7A, HELIOS, SRAC95, TRIFON and UNK) give rather close results for the reaction rates in the UOX fuel cell.

For the MOX fuel cells the MULCOS results were treated as incorrect because of too large discrepancies (up to 4%) in K_{inf} and were not taken into account in further analysis of the results. The maximum deviations in K_{inf} are the same order as in case of the UOX fuel: 1.1–1.3%; the SRAC95 code gives the maximum K_{inf} value. The nature of these discrepancies can be seen from Tables 1.39–1.41 where comparisons of the MOX cell neutron balances are shown. As these tables indicate, more than 90%–contribution to the total absorption is mainly due to ^{239}Pu, ^{238}U, ^{240}Pu and ^{241}Pu (approximately 45, 25, 15 and 8% respectively). Besides, about 30% of the total absorption are due to ^{239}Pu fission. This means that, for instance, 1%–increase in ^{239}Pu fission rate results in at least 0.8%–increase in K_{inf}. Tables 1.39–1.41 demonstrate that the significant overestimation in K_{inf} (1.1–1.3%) by SRAC95 in comparison with HELIOS, may be mainly explained by more than 1.5%–increase in ^{239}Pu fission rate.

In this intercomparison all considered deterministic codes used different cross-sections based on various nuclear data libraries. Besides, energy group structures and resonance self-shielding methods were different too. As reported in [9], problems of preparation of nuclear cross-sections for plutonium nuclides using modern nuclear libraries together with rigorous treatment of resonance self-shielding are essential in MOX fuel calculations.

1.5. Discussions

Analysis of the calculational results for LWR MOX pin cells obtained by the TRIFON and UNK codes as compared with other codes with various cross-sections shows the following:

- Both TRIFON and UNK demonstrate rather good agreement within 1.5σ (where σ is a standard deviation) in K_{inf} calculation; TRIFON slightly overestimates K_{inf} compared with UNK.
- Both TRIFON and UNK predict the reactivity effects with very good accuracy (compared with the mean value):
  - the fuel temperature (Doppler) effect – within 5%;
  - the moderator temperature effect – within 5%;
  - the void effect up to 70% void fraction – within 5-10%;
  - the boron and Xe/Sm poisoning effects – within 4%.
- The UNK code calculates neutron balance within pin cell more precisely in comparison with TRIFON.

At the same time it should be mentioned to the following facts:

- in some cases the Monte Carlo calculations gave very poor accuracy in prediction of the reactivity effects;
- there are significant discrepancies up to 0.5% in K_{inf} calculation using the same code due to “user effect”;
- the SCALE code underestimated K_{inf} value by more than 1% for the VVER cases;
- a problem of rigorous treatment of Pu resonance self-shielding is essential in MOX fuel calculations.

References

1. "Light Water Reactor (LWR) Pin Cell Benchmark Intercomparison," JEFF Report 15, September 1999.
2. W. Bernnat, et al., "Analysis of LWR Benchmarks Based on Different Methods and Nuclear Data Evaluations," Proceedings of the ANS International Topical Meeting on Advances in Reactor Physics and Mathematics and Computation into the Next Millenium (PHYSOR 2000), Pittsburgh, Pennsylvania, USA, May 7-12,2000.
3. H. Takano, et al., "Benchmark Problems on Transmutation Calculation by the OECD/NEA Task Force on Physics Aspects of Different Transmutation Concepts," Proceedings of the International Conference on the Physics of Nuclear Science and Technology, Long Island, NY, USA, October 1998.
4. "Calculations of Different Transmutation Concepts. An International Benchmark Exercise," NEA Nuclear Science Committee, OECD/NEA, February 2000.
5. Neutronics Benchmarks for the Utilization of Mixed-Oxide Fuel: Joint U.S. / Russian Progress Report for Fiscal Year 1997, Volume 3 - Calculations Performed in the Russian Federation, ORNL/TM-13603/V3, June 1998
6. R. J. Ellis, "Analysis of Weapon-Grade MOX VVER-1000 Neutronics Benchmarks: Pin-Cell Calculations with SCALE/SAS2H," ORNL/TM-2000/4, 2000
7. J. C. Gehin, C. Dourougie, M. B. Emmett and R. A. Lillie, "Analysis of Weapon-Grade MOX VVER-1000 Benchmarks with HELIOS and KENO," ORNL/TM-1999/78, July 1999
8. D. H. Hollenbach and P. B. Fox, "Neutronics Benchmarks of Mixed-Oxide Fuels Using the SCALE/CENTRM Sequence," ORNL/TM-1999/299, February 2000
9. "Benchmark Calculations of Power Distribution within Fuel Assemblies. Phase II: Comparison of Data Reduction and Power Reconstruction Methods in Production Codes," NEA/NSC/DOC(2000)3, November 2000

2. LWR CORE CALCULATIONS

2.1. PNL MOX Assemblies

A series of six critical experiments with MOX fuel lattices was performed in the Plutonium Recycle Critical Facility at Pacific Northwest Laboratory in 1975-76. The purpose of these experiments was not only to measure criticality data but also to measure power distribution in selected fuel rods. There are three different lattice pitches, with each pitch used in two problems. Natural UO_2-2% PuO_2 (8% ^{240}Pu) fuel was arranged in a square-pitched lattice with borated or unborated water moderator [1,2]. The critical assemblies are designated PNL-30 through PNL-35 and adopted by the Cross Section Evaluation Working Group for use as criticality safety benchmarks. Main parameters of the benchmark assemblies are given in Table 2.1.

Table 2.1. Parameters of PNL Assemblies

Case	Lattice Pitch (cm)	No. of Fuel Rods	Moderator Temperature (°C)	Soluble Boron (ppm)	Axial Buckling (m^{-2})
PNL-30	1.77800	469	20.98	1.7	9.091
PNL-31	1.77800	761	21.90	687.9	9.381
PNL-32	2.20914	195	22.75	0.9	9.322
PNL-33	2.20914	761	22.66	1090.4	9.487
PNL-34	2.51447	160	22.15	1.6	9.842
PNL-35	2.51447	689	23.40	767.25	9.480

The detailed specifications of these benchmark experiments together with some results of the Monte Carlo calculations are given in [3]. There are two benchmark models: basic 3-D model and simplified 2-D model with uniform axial representation (ignoring the grids, support plates and so on). For the last model the effective assembly height was defined using the experimental value of axial buckling.

In the BARS calculations the 2-D model was used. Calculations were performed using two 5-group cross-section libraries (based on ENDF/B-VI) calculated by TRIFON or UNK.

The assemblies, except for PNL-32, had 1/8-symmetry layout of fuel rods. Configurations of the assemblies are shown in Figures 2.1 and 2.2. Measurements of pin-power distribution were carried out mainly along lines of symmetry X and Y as shown in these figures.

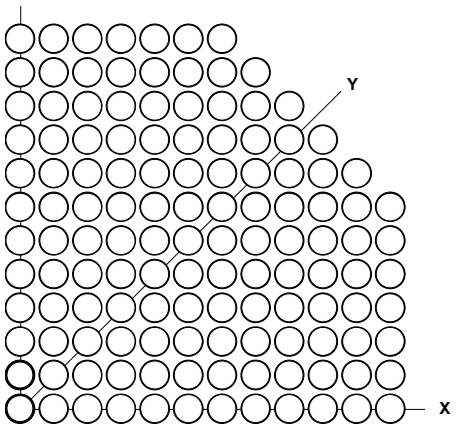

PNL-30

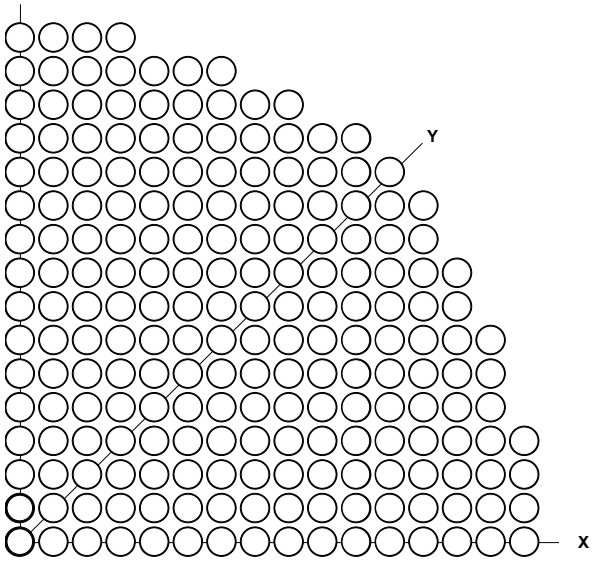

PNL-31

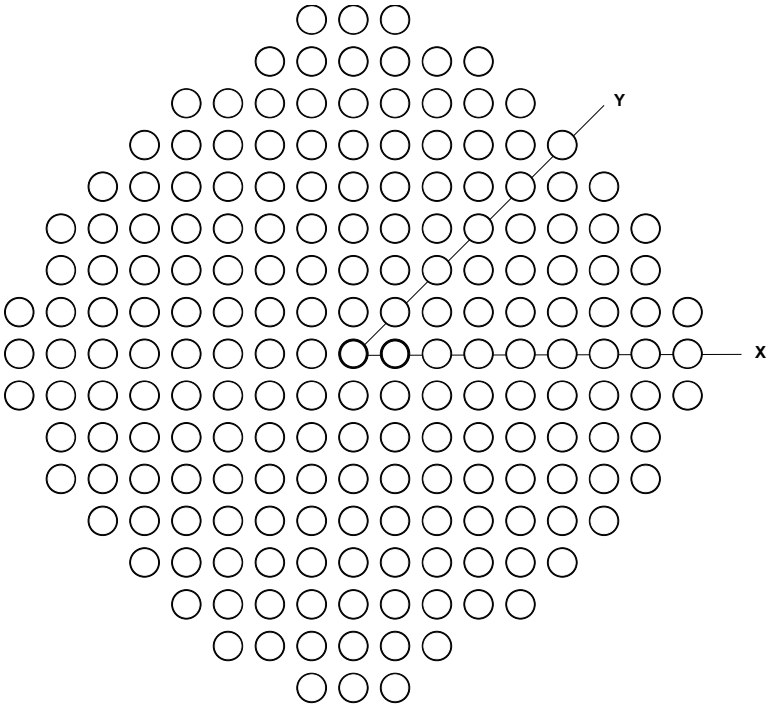

PNL-32

Figure 2.1. Configurations of MOX Assemblies PNL-30 through PNL-32

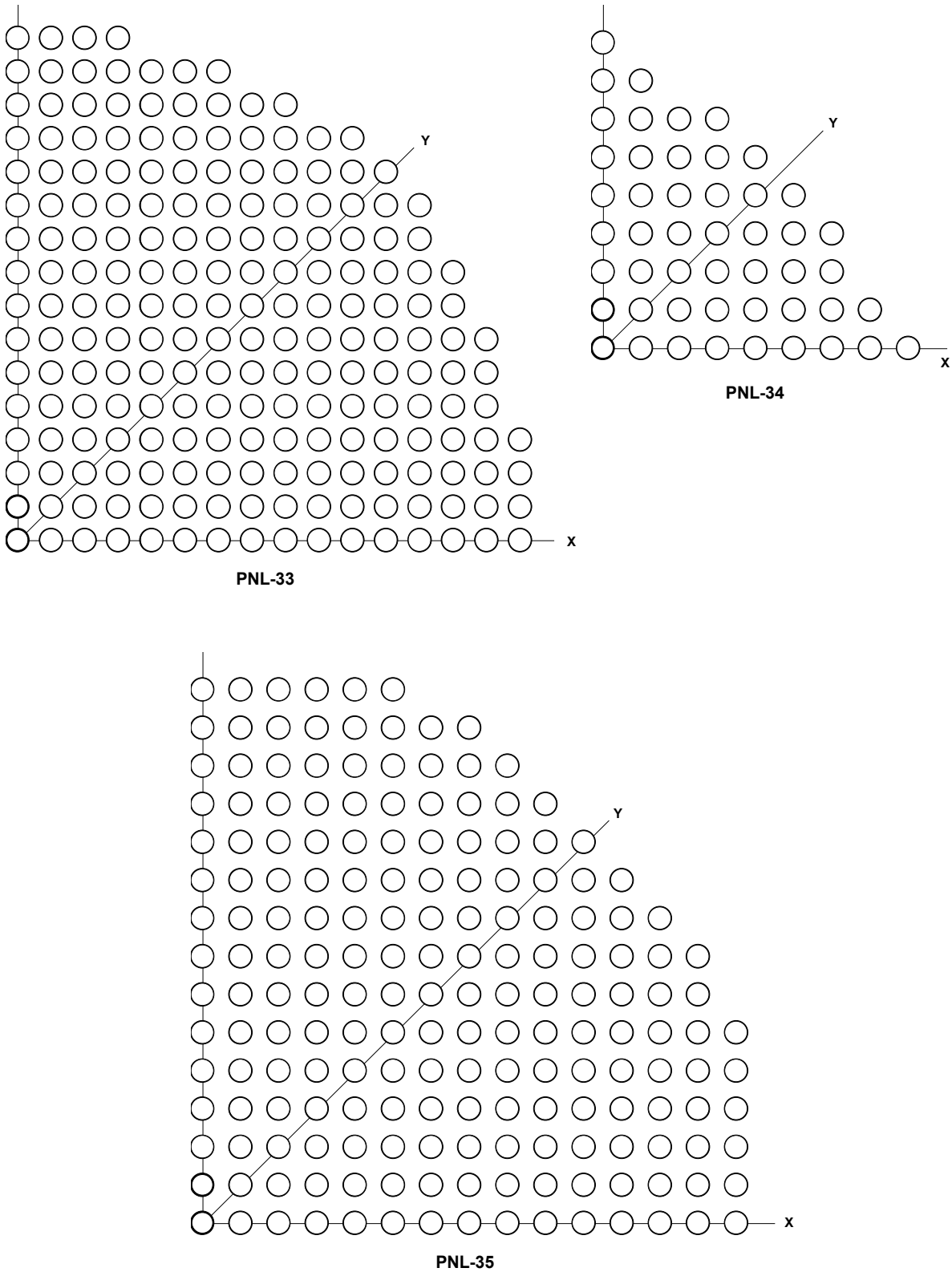

Figure 2.2. Configurations of MOX Assemblies PNL-33 through PNL-35

Comparison of the effective multiplication factor (K_{eff}) calculated by BARS and other codes [3-6] with using different benchmark models and cross-section libraries (based on JEF-2.2, ENDF/B-V, ENDF/B-VI, and JENDL-3.2) are shown in Table 2.2.

Table 2.2. K_{eff} Calculational Results for PNL MOX Assemblies

	PNL-30	PNL-31	PNL-32	PNL-33	PNL-34	PNL-35
Two-Dimensional Modeling						
MCNP-4B [3] (ENDF/B-V)	0.9990 (8)*	0.9996 (9)	1.0031 (9)	1.0071 (8)	1.0061 (8)	1.0077 (8)
MCNP-4B [5] (ENDF/B-V)	1.0013 (7)	1.0051 (8)	1.0071 (7)	1.0130 (7)	1.0111 (7)	1.0134 (7)
MCNP-4B [5] (ENDF/B-VI)	0.9948 (8)	0.9990 (7)	0.9995 (7)	1.0072 (7)	1.0036 (7)	1.0079 (7)
BARS-TRIFON (ENDF/B-VI)	0.99332	0.99898	0.99058	1.00341	0.99364	1.00312
BARS-UNK (ENDF/B-VI)	0.98967	0.99547	0.99098	1.00202	0.99470	1.00197
Three-Dimensional Modeling						
MCNP-4B [3] (ENDF/B-V)	0.9976 (9)	0.9999 (8)	1.0012 (8)	1.0083 (8)	1.0053 (8)	1.0087 (8)
KENO-V [4] (ENDF/B-V)	0.9966 (4)	0.9987 (3)	1.0000 (4)	1.0064 (4)	1.0020 (5)	1.0068 (4)
MCNP-4B [5] (ENDF/B-V)	0.9979 (8)	1.0023 (7)	1.0049 (7)	1.0105 (7)	1.0084 (7)	1.0118 (8)
MCNP-4B [5] (ENDF/B-VI)	0.9917 (7)	0.9968 (7)	0.9970 (7)	1.0042 (7)	1.0018 (7)	1.0061 (7)
MCNP [6] (JEF-2.2)	0.9944	0.9978	0.9961	1.0034	0.9990	1.0007
MCNP [6] (JENDL-3.2)	0.9980	0.9998	1.0009	1.0067	1.0014	1.0069
MCNP [6] (ENDF/B-VI)	0.9900	0.9942	0.9948	1.0020	0.9980	1.0035

* Read as 0.9990 ± 0.0008

Analysis of the pin-by-pin power distributions was carried out using both experimental [1, 2] and calculational [4, 5] data. Number of pin-power measurements per assembly was 19-26. Table 2.3 gives root-mean-square (RMS) deviations between the measured and calculated pin-power distributions. Average RMS deviations for the BARS-TRIFON and BARS-UNK results are 1.49% and 1.44%, respectively. The measured and calculated (by BARS-UNK) pin-power distributions for 4 assemblies are compared in Figure 2.3 along axis X (PNL-31, PNL-34 and PNL-35) and axis Y (PNL-32).

Table 2.3. RMS Deviations (%) from Measured Data in Pin-Power Distribution

	PNL-30	PNL-31	PNL-32	PNL-33	PNL-34	PNL-35
BARS-TRIFON	1.60	1.58	0.94	1.79	1.42	1.48
BARS-UNK	1.53	1.40	0.89	1.65	1.33	1.69

Comparison between calculated data obtained for PNL-34 by BARS and MCNP [5] shows that RMS deviation is less than 0.7% and 0.9% for the MCNP (ENDF/B-V) and MCNP (ENDF/B-VI) cases, respectively. These deviations are less than one standard deviation of the Monte Carlo calculation (σ is about 1%). (It should be noted the following fact: the maximum difference between pin-power distributions calculated by MCNP using ENDF/B-V and ENDF/B-VI was above 3%, i.e. more than 3σ).

Comparison of the pin-by-pin power distributions calculated by BARS and KENO-V (using the SCALE/CENTRM sequence) [4] is shown in Table 2.4. The KENO-V data were obtained with average standard deviation of 0.6-0.7%. All fuel rods were taken into account in this comparison. As shown in Table 2.4, average RMS deviations for the BARS-TRIFON and BARS-UNK results do not exceed 1.2% and 1.0%, respectively.

Table 2.4. RMS Deviations (%) from the KENO-V Data in Pin-Power Distribution

	PNL-30	PNL-31	PNL-32	PNL-33	PNL-34	PNL-35
BARS-TRIFON	1.03	1.35	1.39	1.38	0.92	1.07
BARS-UNK	0.93	1.20	1.14	1.12	0.74	0.87

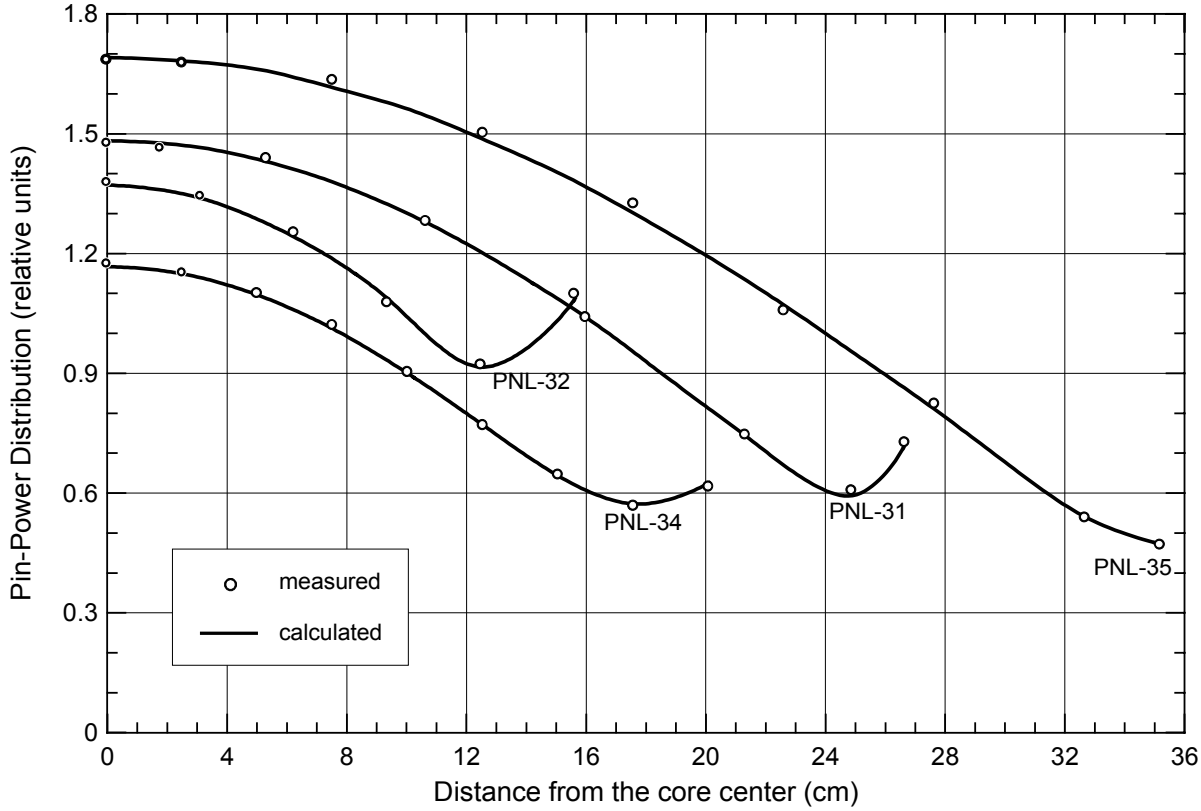

Figure 2.3. Pin-Power Distributions for PNL Assemblies

2.2. Saxton MOX Assemblies

A series of critical experiments with water moderated, single-region and multi-region UO_2-PuO_2 and/or UO_2 fueled cores was performed in the Critical Reactor Experiment facility at the Westinghouse Reactor Evaluation Center in 1965 as part of the Saxton Plutonium Program. The purpose of these experiments was to verify the nuclear design of the Saxton partial plutonium core, which consisted of UO_2-PuO_2 assemblies in the central region with enriched UO_2 peripheral assemblies. Single-region and multi-region MOX/UOX experiments with both natural UO_2-PuO_2 and enriched UO_2 with several different pitched lattices and clean or borated moderator have been performed. A number of significant parameters, such as control rod worths, soluble poison worths, pin-power distribution and voiding effects were investigated during these experiments.

Here only six single-region square-pitched lattices, consisting in natural UO_2-6.6 wt.% PuO_2 mixed-oxide fuel, with five different pitches, are considered. The experiments with 1.4224-cm pitched lattices were performed with borated (337 ppm of soluble boron) or pure water moderator. Other pitched-lattice experiments (with 1.3208-cm, 1.8679-cm, 2.0116-cm and 2.6416-cm pitches) were performed only with pure water moderator. All of these were judged to be acceptable as benchmark data [7]. Main parameters of these benchmark assemblies designated as SAXTON-1 through SAXTON-6 are given in Table 2.5.

Table 2.5. Parameters of Selected Single-Region Assemblies

Case	Lattice Pitch (cm)	Core Configuration	Moderator Temperature (°C)	Soluble Boron (ppm)	Axial Buckling (m^{-2})
SAXTON-1	1.3208	22×23	25.8	0	10.7
SAXTON-2	1.4224	19×19	15.8	0	11.1
SAXTON-3	1.4224	21×21	18.0	337	9.64
SAXTON-4	1.8679	13×13	24.1	0	16.1
SAXTON-5	2.0116	12×12	16.1	0	13.4
SAXTON-6	2.6416	11×11	19.9	0	12.5

The detailed specifications of these benchmark experiments together with some results of the Monte Carlo calculations are given in [7]. There are two benchmark models: basic 3-D model and simplified 2-D model with uniform axial representation (ignoring the grids, support plates and so on). For the last model the effective assembly height was defined using the experimental value of axial buckling.

In the BARS calculations the 2-D model was used. Calculations were performed using two 5-group cross-section libraries (based on ENDF/B-VI) calculated by TRIFON or UNK.

All assemblies had very simple layout of fuel rods. Their configurations are shown in Figure 2.4, where for SAXTON-2 axis X was chosen for comparison of the BARS calculational pin-power distribution with the measured data [8] and the KENO-V calculation [4].

Comparison of the effective multiplication factor (K_{eff}) calculated by BARS and other codes [4,6-10] are presented in Table 2.6. Analysis of obtained data shows, that the mean values of K_{eff} calculated by BARS-TRIFON and BARS-UNK are lower by 1% compared with those calculated by the Monte Carlo codes. On the other hand, the MCNP-4B results obtained for a 3-D model with using two libraries (ENDF/B-V and ENDF/B-VI), show that the last values (obtained with ENDF/B-VI) are lower by 0.6-0.8%. Note here, that the WIMS-D4M+DIF3D complex overestimates K_{eff} by 1-2%.

The pin-by-pin power distributions calculated by the BARS-TRIFON and BARS-UNK codes were compared using mainly the KENO-V calculational data [4]. The KENO-V (with using the SCALE/CENTRM sequence) data were obtained with averaged standard deviation of order of 0.6-0.8%. All fuel rods were taken into account in this comparison. Table 2.7 shows root-mean-square deviations between the BARS and KENO-V pin-power distributions. Average RMS deviations for the BARS-TRIFON and BARS-UNK results are 1.25% and 0.97%, respectively.

A single comparison between the measured and BARS calculational pin-power distributions for SAXTON-2 shows that RMS deviation is 0.83% (there are only 13 measured fuel rods). Figure 2.5 presents the SAXTON-2 pin-power distributions (along axis X) obtained from measurements and calculated by the BARS and KENO-V codes.

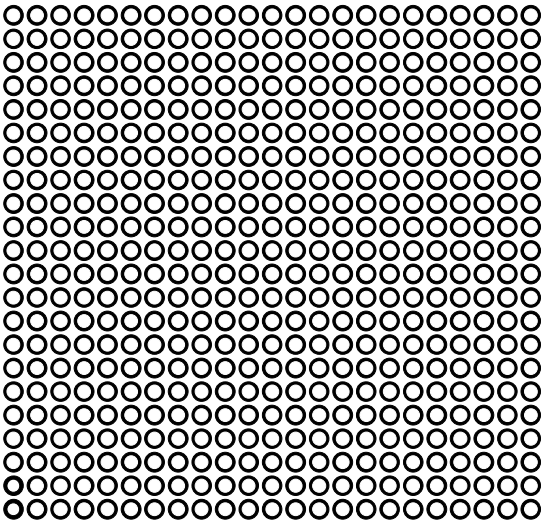

SAXTON-1 (23 x 22)

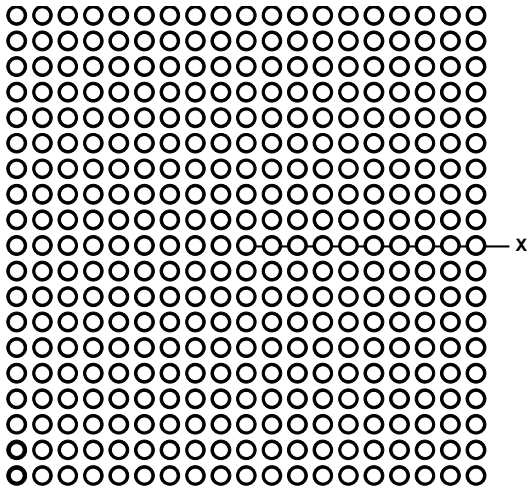

SAXTON-2 (19 x 19)

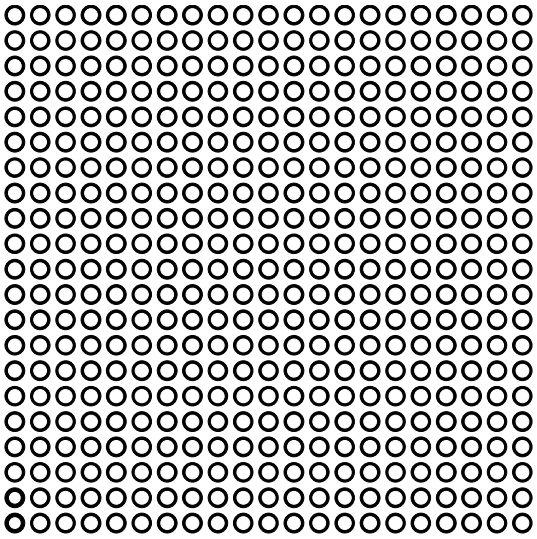

SAXTON-3 (21 x 21)

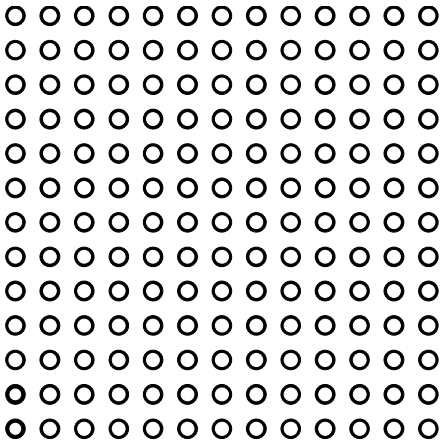

SAXTON-4 (13 x 13)

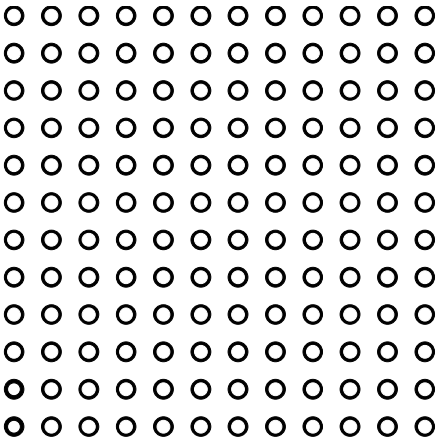

SAXTON-5 (12 x 12)

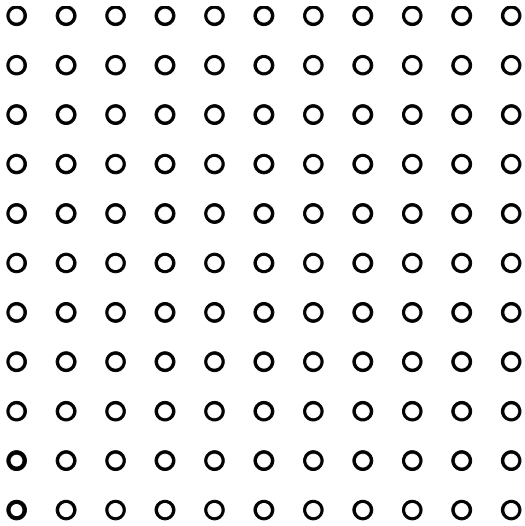

SAXTON-6 (11 x 11)

Figure 2.4. Configurations of MOX Assemblies SAXTON-1 through SAXTON-6

Table 2.6. K_{eff} Calculational Results for Saxton Assemblies

	SAXTON-1	SAXTON-2	SAXTON-3	SAXTON-4	SAXTON-5	SAXTON-6
Two-Dimensional Modeling						
MCNP-4B [7] (ENDF/B-V)	0.9983(9)*	1.0008(9)	0.9993(9)	1.0042(10)	1.0062(9)	1.0065(10)
WIMS-D4M + DIF3D [9]	1.00809	1.00179	1.01034	1.01959	1.01891	1.02385
WIMS-7A [10] (JEF 2.2)	1.00443	1.00070	0.99895	0.99142	0.99425	0.99181
BARS-TRIFON (ENDF/B-VI)	0.99110	0.98999	0.99208	0.98374	0.98382	0.99053
BARS-UNK (ENDF/B-VI)	0.98612	0.98728	0.98906	0.98625	0.98685	0.99224
Three-Dimensional Modeling						
MCNP-4B [7] (ENDF/B-V)	0.9955(9)	0.9989(9)	0.9988(9)	1.0015(8)	1.0013(9)	1.0061(9)
MONK8A [7] (JEF 2.2)	0.9943(10)	0.9979(10)	0.9957(10)	0.9976(10)	0.9980(10)	0.9974(10)
MCNP-4B [8] (ENDF/B-V)	0.9972(5)	0.9995(3)	0.9997(5)	1.0041(5)	1.0057(5)	1.0071(5)
MCNP-4B [8] (ENDF/B-VI)	0.9915(5)	0.9936(3)	0.9930(5)	0.9964(5)	0.9977(5)	0.9997(5)
KENO-V [4] (ENDF/B-V)	1.0007(4)	1.0012(4)	1.0017(4)	1.0029(4)	1.0035(4)	1.0059(4)
MCNP [6] (JEF-2.2)	0.9949	0.9955	0.9941	0.9948	0.9959	0.9992
MCNP [6] (JENDL-3.2)	0.9991	1.0003	0.9997	0.9996	0.9994	1.0024
MCNP [6] (ENDF/B-VI)	0.9933	0.9939	0.9942	0.9947	0.9952	0.9980

* Read as 0.9983 ± 0.0009

Table 2.7. RMS Deviations (%) from the KENO-V Data in Pin-Power Distribution

	SAXTON-1	SAXTON-2	SAXTON-3	SAXTON-4	SAXTON-5	SAXTON-6
BARS-TRIFON	1.14	0.98	0.91	1.55	1.29	1.61
BARS-UNK	1.13	0.67	0.64	1.14	0.82	1.44

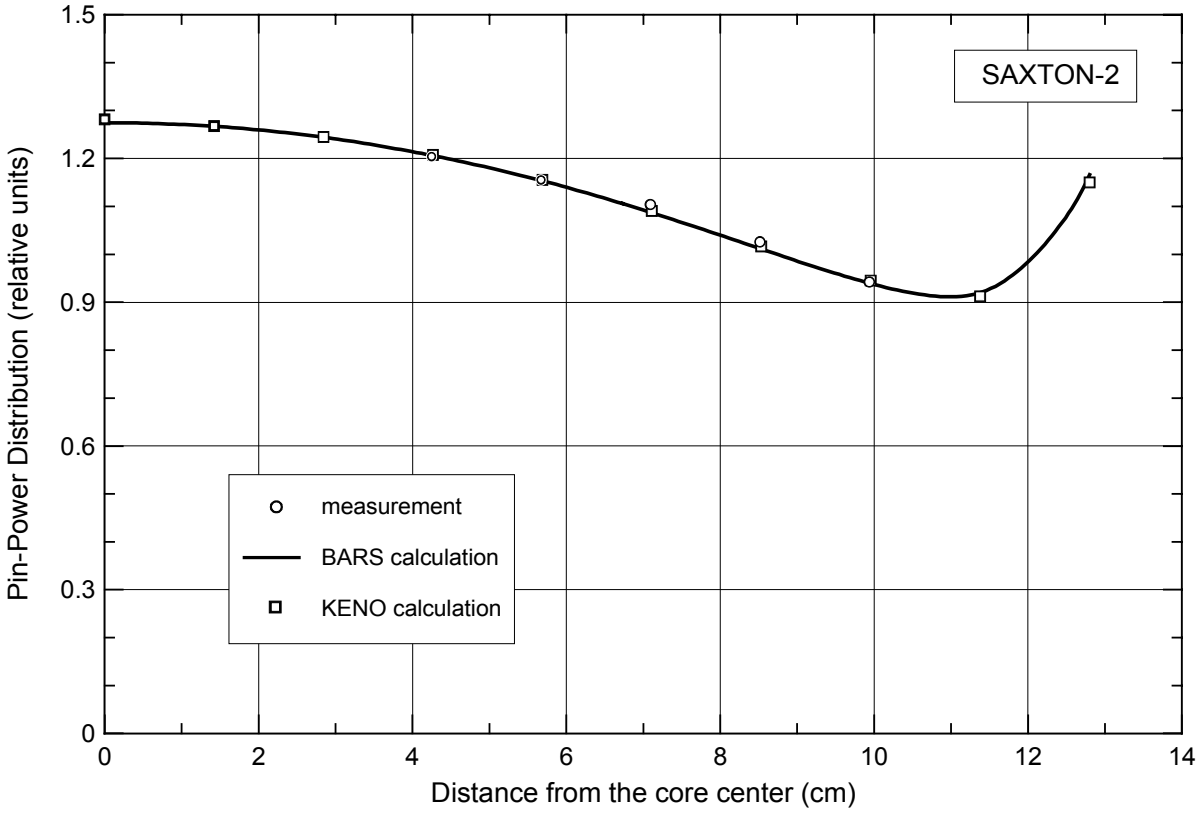

Figure 2.5. Pin-Power Distributions for SAXTON-2

2.3. TCA MOX Assemblies

The experiments were performed between 1972 and 1975 at Tokai Research Establishment of JAERI at the Tank-Type Critical Assembly (TCA). TCA is a light-water-moderated critical assembly with 3.01 wt.% PuO_2 – natural UO_2 fuel rods in square lattice. The water-to-fuel volume ratio in the lattice cells ranged from 2.42 to 5.55. The critical water level and total critical buckling of the experimental cores were measured at temperature from 10 to 30°C. Some physics parameters, such as temperature coefficient of reactivity, the extrapolation length, and critical buckling, were also investigated. Eleven configurations are judged to be acceptable as benchmark data [11]. Main parameters of selected benchmark assemblies designated as TCA-1 through TCA-11 are given in Table 2.8.

Table 2.8. Parameters of TCA Assemblies

Lattice Name	Lattice Pitch (cm)	Core Configuration	Extrapolation Length (cm)	Case No.	Critical Level at 20 °C (cm)
2.42PU	1.825	23 × 23	12.5	TCA-1	59.55
				TCA-2	61.90
				TCA-3	64.06
2.98PU	1.956	21 × 21	12.0	TCA-4	61.50
				TCA-5	64.40
				TCA-6	69.40
4.24PU	2.225	20 × 20	11.6	TCA-7	60.32
				TCA-8	62.99
				TCA-9	65.63
5.55PU	2.474	21 × 21	11.3	TCA-10	62.05
				TCA-11	64.53

There are four types of the fuel lattice configurations as shown in Figure 2.6, where axis X was chosen for comparison between the BARS calculational pin-power distribution and the KENO-V calculation [4].

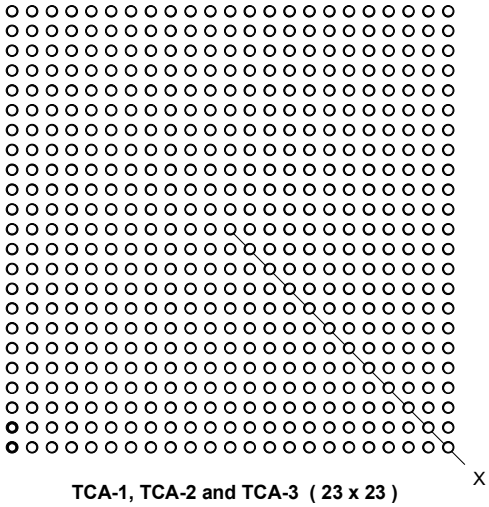

TCA-1, TCA-2 and TCA-3 (23 x 23)

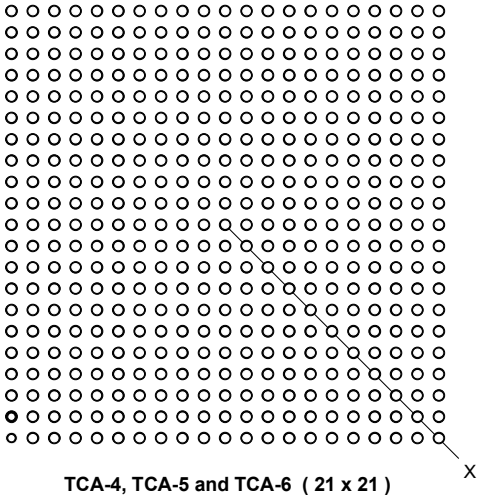

TCA-4, TCA-5 and TCA-6 (21 x 21)

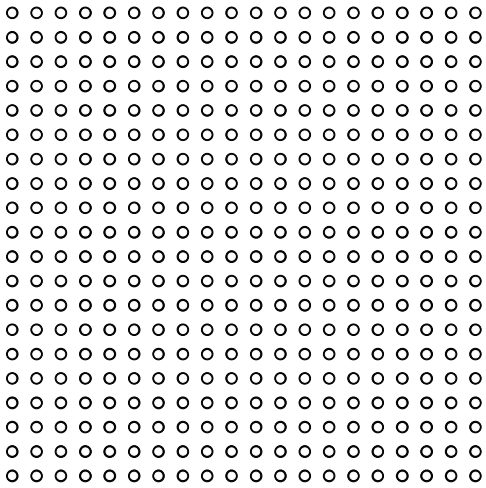

TCA-7, TCA-8 and TCA-9 (20 x 20)

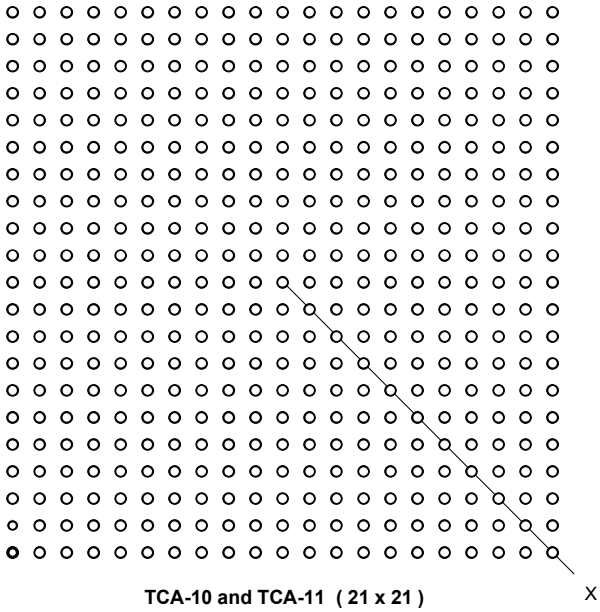

TCA-10 and TCA-11 (21 x 21)

Figure 2.6. Configurations of TCA Lattices Types

The detailed specifications of these benchmark experiments together with some results of the Monte Carlo calculations are given in [11]. There are two benchmark models: basic 3-D model and simplified 2-D model with uniform axial representation (ignoring the grids, support plates and so on), for which the effective assembly height was defined using the experimental value of extrapolation length.

In the BARS calculations the 2-D model was used. Calculations were performed using two 5-group cross-section libraries (based on ENDF/B-VI) calculated by the TRIFON or UNK codes. Comparison of the effective multiplication factor (K_{eff}) calculated by BARS and other codes [4,6,11] used 3-D model, are presented in Tables 2.9 and 2.10.

Table 2.9. K_{eff} Calculational Results for TCA Assemblies (Part I)

Case No.	MCNP-4B [11] (JENDL-3.2)	KENO-V [11] (JENDL-3.2)	MONK7B [11] (JEF-2.2)	KENO-V [4] (ENDF/B-V)
TCA-1	0.9925(11)*	1.0172(11)	0.9992(10)	0.9963 (5)
TCA-2	0.9971(11)	1.0149(10)	1.0002(10)	0.9969 (4)
TCA-3	0.9950(11)	1.0170(10)	0.9998(10)	0.9985 (5)
TCA-4	0.9990(10)	1.0092(10)	0.9986(10)	0.9973 (4)
TCA-5	0.9973(10)	1.0090 (9)	1.0020(10)	0.9982 (4)
TCA-6	0.9974(11)	1.0098(10)	1.0014(10)	0.9988 (4)
TCA-7	0.9972 (9)	1.0007(10)	1.0023(10)	0.9994 (4)
TCA-8	0.9973(10)	1.0022(10)	0.9987(10)	1.0002 (4)
TCA-9	0.9994(10)	1.0029(10)	0.9998(10)	1.0009 (4)
TCA-10	0.9990 (9)	0.9959 (9)	1.0006(10)	1.0003 (3)
TCA-11	0.9999 (9)	0.9991 (9)	0.9988(10)	1.0010 (4)

* Read as 0.9925 ± 0.0011

Table 2.10. K_{eff} Calculational Results for TCA Assemblies (Part II)

Case No.	BARS-TRIFON (ENDF/B-VI)	BARS-UNK (ENDF/B-VI)	MCNP [6] (JEF-2.2)	MCNP [6] (JENDL-3.2)
TCA-1	0.98582	0.98574	0.9930	0.9926
TCA-2	0.98707	0.98692	0.9946	0.9972
TCA-3	0.98757	0.98736	0.9946	0.9950
TCA-4	0.98670	0.98713	0.9936	0.9991
TCA-5	0.98812	0.98848	0.9949	0.9974
TCA-6	0.98908	0.98932	0.9951	0.9975
TCA-7	0.99064	0.99248	0.9948	0.9973
TCA-8	0.99136	0.99483	0.9949	0.9975
TCA-9	0.99215	0.99223	0.9960	0.9995
TCA-10	0.99510	0.99443	0.9954	0.9990
TCA-11	0.99525	0.99455	0.9944	0.9999

Comparison of the pin-by-pin power distributions was carried out using only the KENO-V calculational data [4]. The KENO-V (with using the SCALE/CENTRM sequence) data were obtained with the standard deviation of about 0.7%. All fuel rods were taken into account in the comparison. Table 2.11 gives root-mean-square (RMS) deviations between the BARS and KENO-V pin-power distributions. Average RMS deviations for the BARS-TRIFON and BARS-UNK results are 1.34% and 1.10%, respectively.

Figure 2.7 presents the pin-power distributions (along axis X) calculated by the BARS and KENO-V codes for TCA-3, TCA-5, and TCA-10.

Table 2.11. RMS Deviations (%) from the KENO-V Data in Pin-Power Distribution

	TCA-1	TCA-2	TCA-3	TCA-4	TCA-5	TCA-6
BARS-TRIFON	1.51	1.39	1.33	1.38	1.61	1.67
BARS-UNK	1.14	0.99	0.97	1.03	1.32	1.37

	TCA-7	TCA-8	TCA-9	TCA-10	TCA-11
BARS-TRIFON	1.27	1.21	1.09	0.91	1.11
BARS-UNK	1.17	1.18	0.89	0.82	1.09

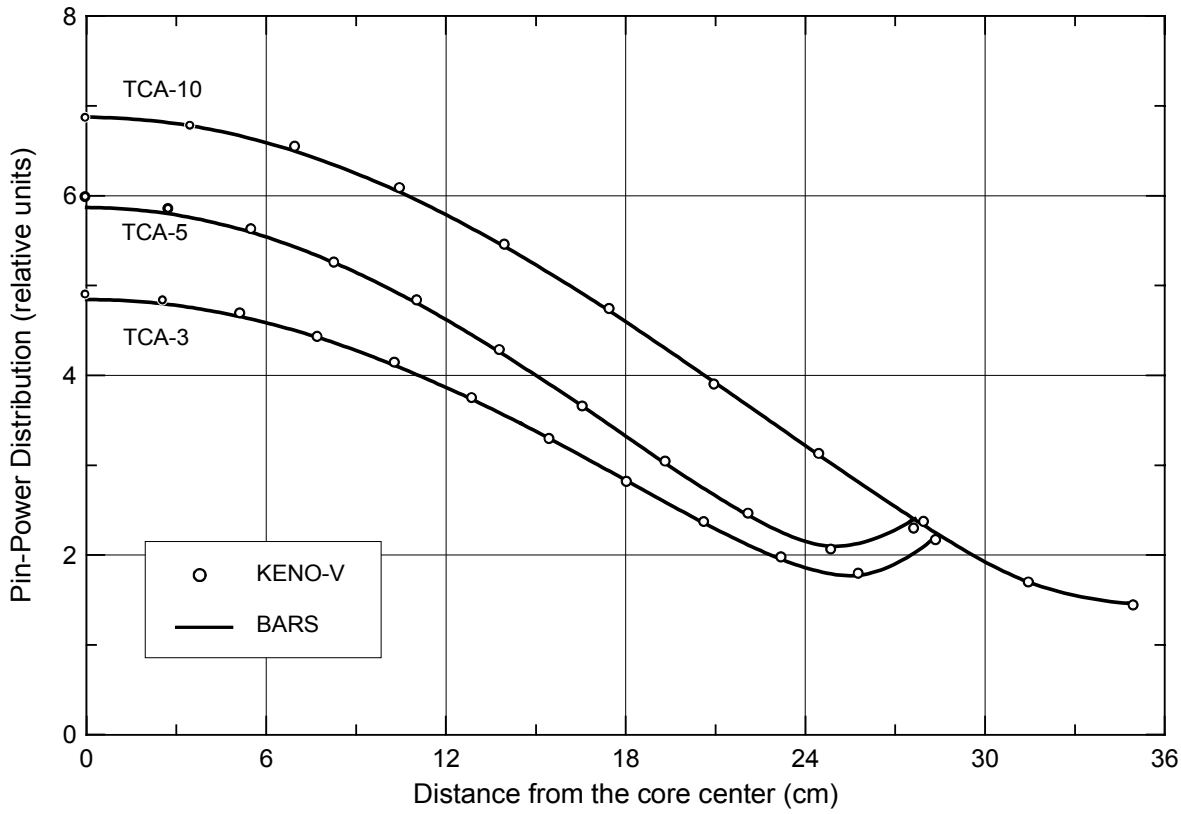

Figure 2.7. Pin-Power Distributions for TCA-3, TCA-5, and TCA-10

2.4. ESADA MOX Assemblies

A series of critical experiments with mixed-oxide and UO_2 fuels in various configurations were performed at the Westinghouse Reactor Evaluation Center (WREC) in 1967 [12]. The experiments were carried out under the joint sponsorship of the Empire State Atomic Development Associates (ESADA) plutonium program and Westinghouse. Three different fuels were used during the experimental program: two MOX fuels and a low-enriched UO_2 fuel. The MOX fuels were distinguished by their ^{240}Pu content: 8-wt.% and 24-wt.% ^{240}Pu. Both MOX fuels contained 2-wt.% PuO_2 in natural UO_2. The UO_2 fuel with 2.72-wt.% enrichment was used for comparison with the plutonium data and for use in multiregion experiments.

A total of 88 different critical core configurations including both single-region and multiregion assemblies were constructed during the ESADA experiments. The lattice pitch, layout, and fuel isotopic composition were varied. The number of single-region experiments was 53. The number of multiregion core configurations, where reactivity worth and power distribution measurements were performed, was 35. They were constructed in three ways: concentric-region core configurations, salt-and-pepper core configurations, and a third configuration that can be generally described as two rectangular slabs loaded with UO_2, sandwiching a center region loaded with MOX fuel.

Concentric-region configurations used two different fuels in the inner and outer regions of the core with various combinations of the available fuels. Eight different core configurations were constructed in this way. Four configurations used 24-wt.% ^{240}Pu in the inner region and 8-wt.% ^{240}Pu in the outer region. Two of these four experiments were performed for a 1.7526-cm lattice pitch. A third experiment was performed for a 1.9050-cm lattice pitch. In addition to the MOX configurations, four additional configurations were constructed by using MOX and UO_2 fuels in a 1.7526-cm lattice. Three core configurations used 24-wt.% ^{240}Pu and UO_2 fuel with different loading patterns. For two of those cases, UO_2 was loaded in the inner region; for one case, MOX fuel was loaded in the inner region. Moreover, one configuration with an 8-wt.% ^{240}Pu inner region and UO_2 outer region was also constructed.

Salt-and-pepper core configurations had a checkerboard pattern for loading two different fuels. All available fuel types were used in various combinations for the salt-and-pepper configurations only with a 1.7526-cm lattice pitch.

The critical water levels for the experimental cores were measured at a room temperature. This section deals mainly with concentric-region and salt-and-pepper core configurations. Main parameters of the selected benchmark assemblies are given in Table 2.12.

Table 2.12. Parameters of ESADA Assemblies

Configuration Core Type	Case Number	Fuel Type	Lattice Pitch (cm)	Number of Fuel Rods	Critical Level (cm)
Single-region	P06	24% ^{240}Pu	2.6942	300	62.62
Concentric-region	P15-10	8% ^{240}Pu / UO_2	1.7526	225 / 400	50.43
	P16-12	24% ^{240}Pu / UO_2	1.7526	225 / 400	79.53
	P17-14	24% ^{240}Pu / 8% ^{240}Pu	1.7526	225 / 492	93.48
	P18-11	UO_2 / 24% ^{240}Pu	1.7526	225 / 400	50.08
	P19-13	24% ^{240}Pu / UO_2	1.7526	121 / 408	74.76
	P20-15	24% ^{240}Pu / 8% ^{240}Pu	1.7526	221 / 468	95.36
	P21-16	24% ^{240}Pu / 8% ^{240}Pu	1.9050	157 / 264	92.65
	P22-17	24% ^{240}Pu / 8% ^{240}Pu	1.9050*	89 / 143	93.42
Salt-and-Pepper	P23-04	8% ^{240}Pu / 24% ^{240}Pu	1.7526	365 / 364	89.18
	P24-05	8% ^{240}Pu / UO_2	1.7526	265 / 264	49.90
	P25-06	24% ^{240}Pu / UO_2	1.7526	265 / 264	89.64
	P26-07	24% ^{240}Pu / UO_2	1.7526	288 / 288	73.42
	P27-08	24% ^{240}Pu / UO_2	1.7526	313 / 312	63.49
	P28-09	24% ^{240}Pu / UO_2	1.7526	249 / 256	93.69

*Outer region had a 2.6942-cm lattice pitch (increased by a factor of $\sqrt{2}$)

Case notation is given using two numbers: first (with letter “P”) - according to numbering in [12] and second - according to numbering in [13]. There were two types of fuels with the same lattice pitch for the concentric-region and salt-and-pepper cases. But in case P22-17 two different lattices were used for the inner and outer regions. Examples of types of the core configurations are shown in Figure 2.8.

The detailed specifications of these benchmark experiments together with some results of the Monte Carlo calculations are given in [12-15].

In the BARS calculations a simplified 2-D model with uniform axial representation was used. Calculations were performed using two 5-group cross-section libraries (based on ENDF/B-VI) calculated by TRIFON or UNK. Comparison of the effective multiplication factor (K_{eff}) calculated by BARS and other codes [13-15] used 3-D model, are presented in Table 2.13.

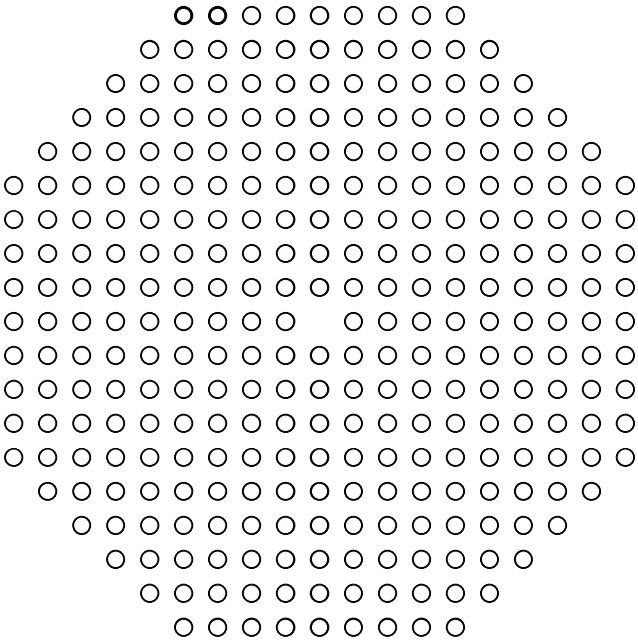

Single-Region Configuration
Case P06

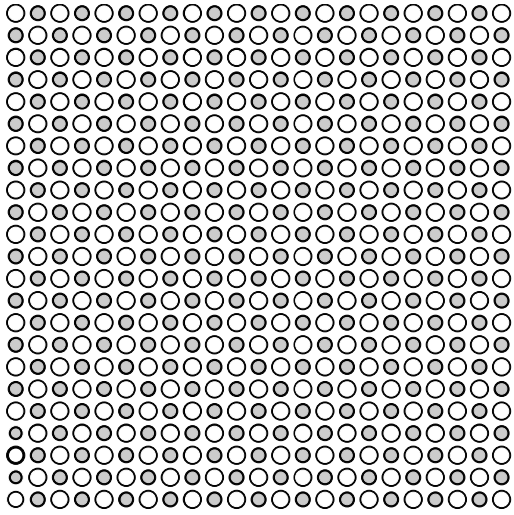

Salt-and-Pepper Configuration
Cases P24-05 and P25-06

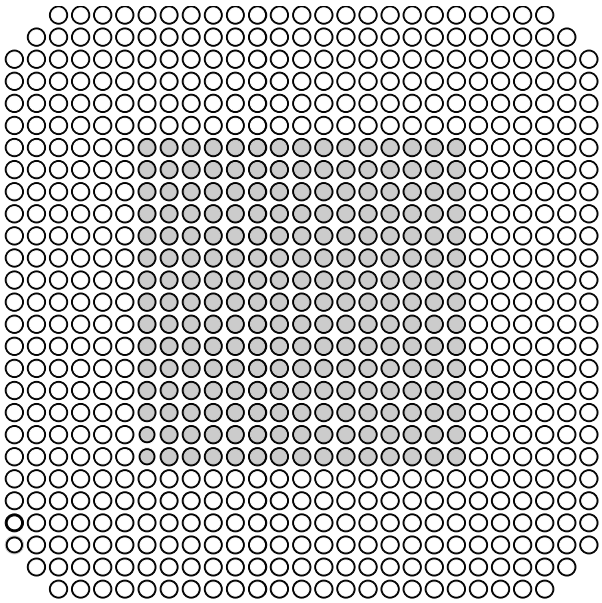

Concentric-Region Configuration
Case P17-14

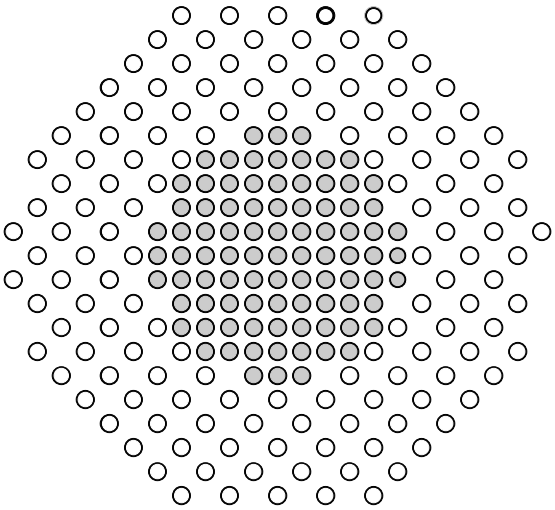

Concentric-Region Configuration
Case P22-17

Figure 2.8. Some Configurations of ESADA Lattice Types

Table 2.13. K_{eff} Calculational Results for ESADA Assemblies

Case No.	MCNP-4A [13] (ENDF/B-VI)	MCNP-4A [13] (ENDF/B-V)	BARS-TRIFON (ENDF/B-VI)	BARS-UNK (ENDF/B-VI)
P06*	1.00200 (60)**	1.00896 (60)	1.00525	1.00398
P15-10	0.98835 (70)	0.99389 (70)	0.99126	0.99139
P16-12	0.99028 (70)	0.99591 (70)	0.99646	0.99632
P17-14	0.98817 (70)	0.99298 (70)	0.99788	0.99315
P18-11	0.99190 (70)	0.99520 (70)	0.99330	0.99478
P19-13	0.99031 (70)	0.99477 (70)	0.99431	0.99608
P20-15	0.98797 (60)	0.99278 (60)	0.99810	0.99335
P21-16	0.99266 (70)	0.99684 (70)	0.99841	0.99549
P22-17	0.99572 (60)	1.00155 (60)	0.99797	0.99525
P23-04	0.99001 (60)	0.99623 (70)	0.99980	0.99490
P24-05	0.98768 (60)	0.99272 (70)	0.98957	0.98974
P25-06	0.99233 (70)	0.99770 (70)	1.00265	1.00182
P26-07	0.99203 (70)	0.99778 (70)	1.00372	1.00273
P27-08	0.99143 (70)	0.99614 (60)	1.00383	1.00272
P28-09	0.99271 (60)	0.99667 (60)	1.00286	1.00204

*MCNP data are taken from [14]

**Read as 1.00200 ± 0.00060

2.5. KRITZ Reactor Series

The KRITZ reactor experiments on regular light water lattices at temperatures up to 245°C, were carried out at Studsvik during the first half of the seventies. Most of the KRITZ series measurements are still not openly accessible. But, recently, data and results for three KRITZ experiments, two of which for UO_2 (1.86 wt.%) rods and one with MOX (1.5 wt.% PuO_2, 91.5% ^{239}Pu) rods, have been released [16]. These included critical experiments at room temperature and high temperature (about 245°C). Fission rate distributions obtained from gamma scanning measurements on irradiated fuel rods are also provided. Main parameters for the three KRITZ regular cores designated as 2:1, 2:13, and 2:19 are given in Table 2.14.

Table 2.14. Parameters of KRITZ Cores

Core Name	Rod Type	Core Configuration	Pitch (cm)	Temperature (°C)	Boron (ppm)	Critical Level (cm)
2:1	UO_2	44×44	1.485	19.7	217.9	65.28
				248.5	26.2	105.52
2:13	UO_2	40×40	1.635	22.1	451.9	96.17
				243.0	280.1	110.96
2:19	MOX	25×24	1.800	21.1	4.8	66.56
				235.9	5.2	100.01

The core configurations are presented in Figure 2.9, where X and Y show the directions of gamma measurements on pin-power distribution.

The simplified specifications for these benchmark experiments are given in [16]. The BARS calculations were performed using a 2-D model. Within this model the effective core height was defined using the experimental value of axial buckling. Calculations were performed using two 5-group cross-section libraries (both based on ENDF/B-VI) calculated by the TRIFON or UNK codes. Comparison of the effective multiplication factor (K_{eff}) calculated by BARS and MCNP using various libraries [6] are presented in Table 2.15.

Comparison of the pin-by-pin power distributions was carried out using experimental data on gamma scanning measurement [16]. Table 2.16 presents root-mean-square (RMS) deviations between the BARS and experimental pin-power distributions.

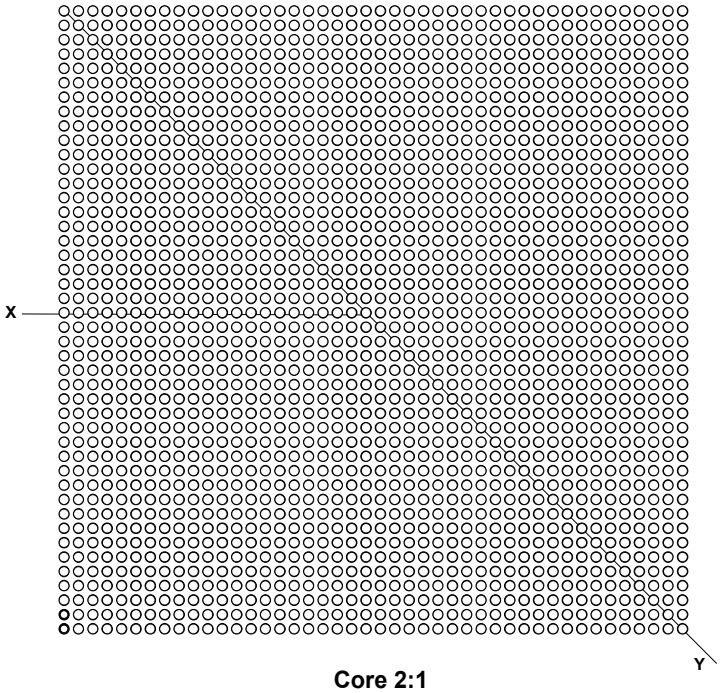

Core 2:1

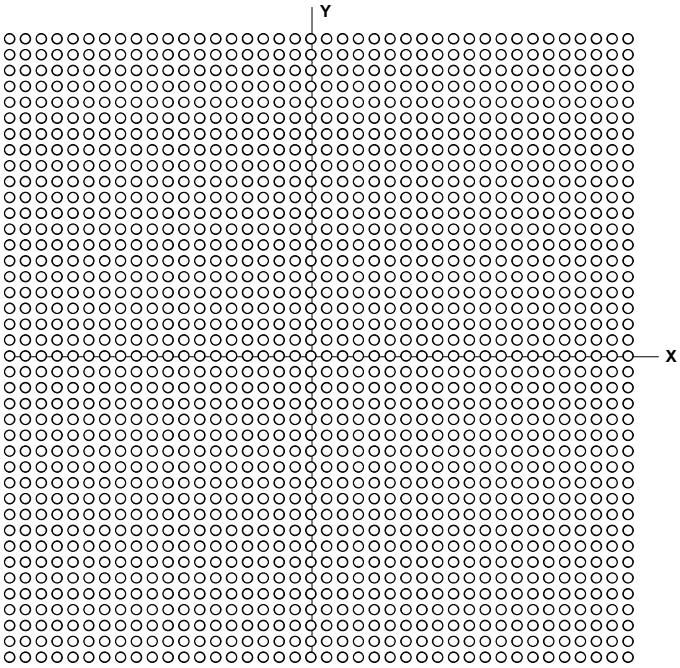

Core 2:13

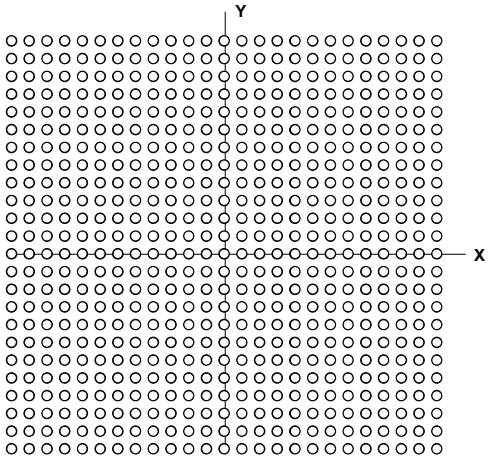

Core 2:19

Figure 2.9. Configurations of KRITZ Cores

Table 2.15. K_{eff} Calculational Results for KRITZ Cores

Core Name	2:1		2:13		2:19	
Temperature (°C)	19.7	248.5	22.1	243.0	21.1	235.9
MCNP (JEF-2.2)	0.9954	0.9928	0.9970	0.9949	0.9966	0.9923
MCNP (ENDF/B-VI)	0.9927	0.9883	0.9950	0.9927	0.9968	0.9941
MCNP (JEFF-3.0)	0.9934	0.9892	0.9957	0.9927	0.9980	0.9954
MCNP (JENDL-3.2)	0.9973	0.9948	0.9998	0.9986	1.0007	0.9980
BARS-TRIFON	1.00250	0.99632	1.00234	0.99926	0.99538	0.99010
BARS-UNK	1.00226	0.99608	1.00290	0.99997	0.99561	0.99027

Table 2.16. RMS Deviations (%) from the Measured Pin-Power Distribution

Core Name	2:1		2:13		2:19	
Temperature (°C)	19.7	248.5	22.1	243.0	21.1	235.9
BARS-TRIFON	-	4.22	1.59	1.95	1.43	1.60
BARS-UNK	-	3.89	1.86	2.39	1.28	1.48

Pin-power distributions (along X and Y directions) calculated by BARS compared with the measured data are presented in Figures 2.10 through 2.12. As shown from Figure 2.10, there are significant discrepancies between the BARS results and the measurements: BARS overestimates pin power by 3% at the central part and up to 9% at the edge of the core, but underestimates power for the corner pins by 5-8%. Such discrepancies may be explained, in particular, by asymmetry in arrangement of Core 2:1 within the experimental tank. There was only 8-cm moderator/reflector layer between the tank walls and two sides of the core. The measured values for 4 symmetrical pins differ up to 7%. The BARS results were obtained with symmetrical arrangement of the core: the reflector thickness was more than 10 cm.

Thus, if do not take the data for Core 2:1 into account, average RMS deviations for the BARS-TRIFON and BARS-UNK results are 1.64% and 1.75%, respectively.

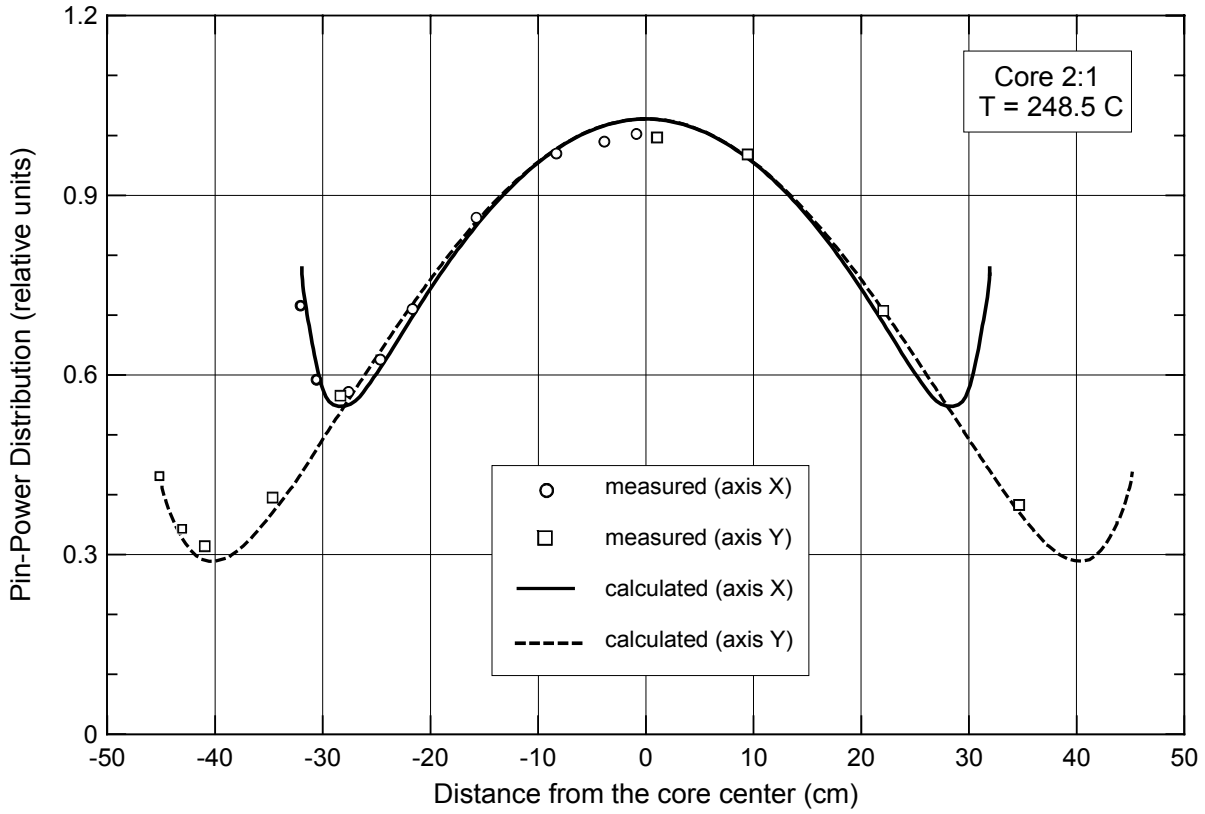

Figure 2.10. Pin-Power Distributions for KRITZ Core 2:1

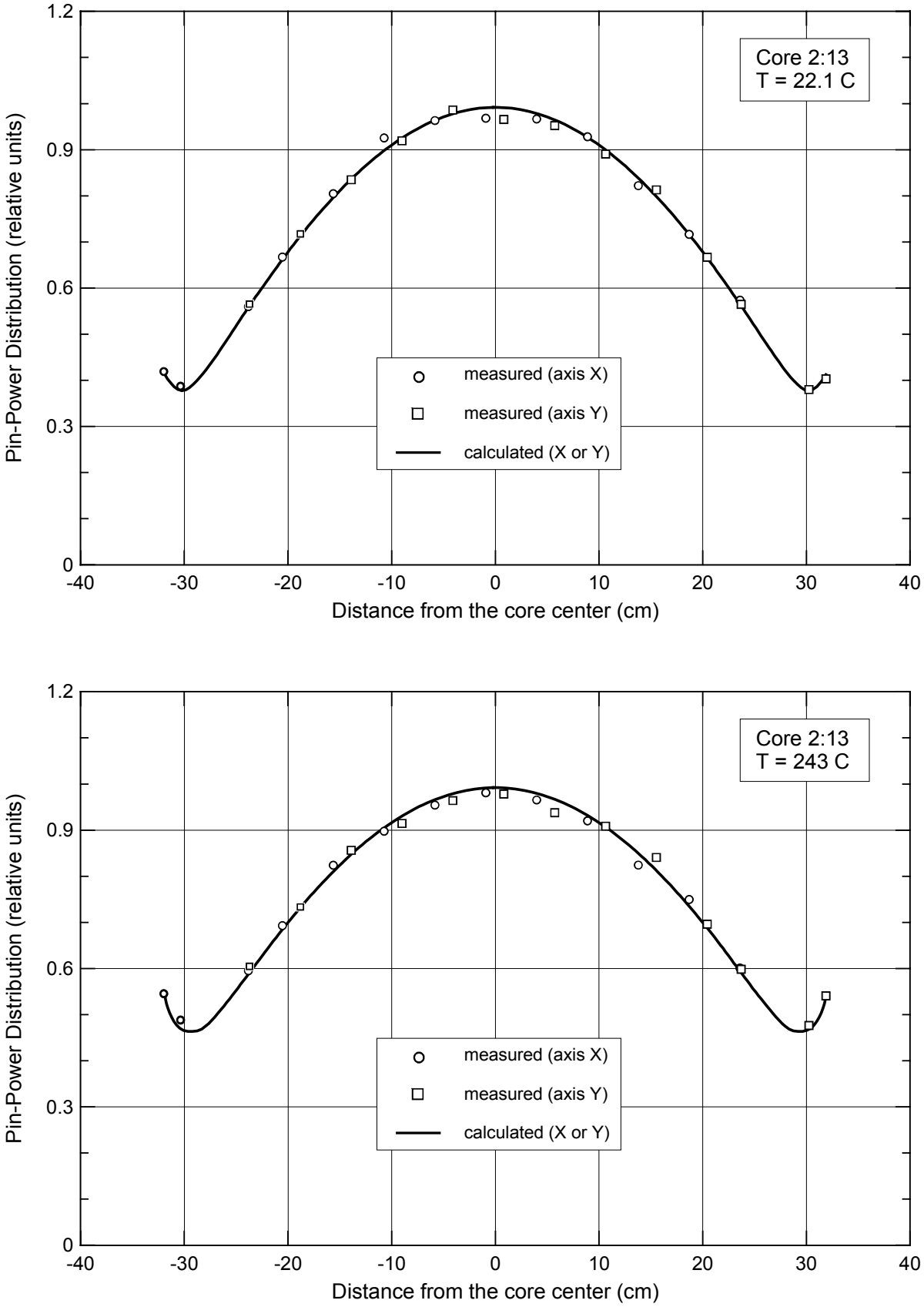

Figure 2.11. Pin-Power Distributions for KRITZ Core 2:13

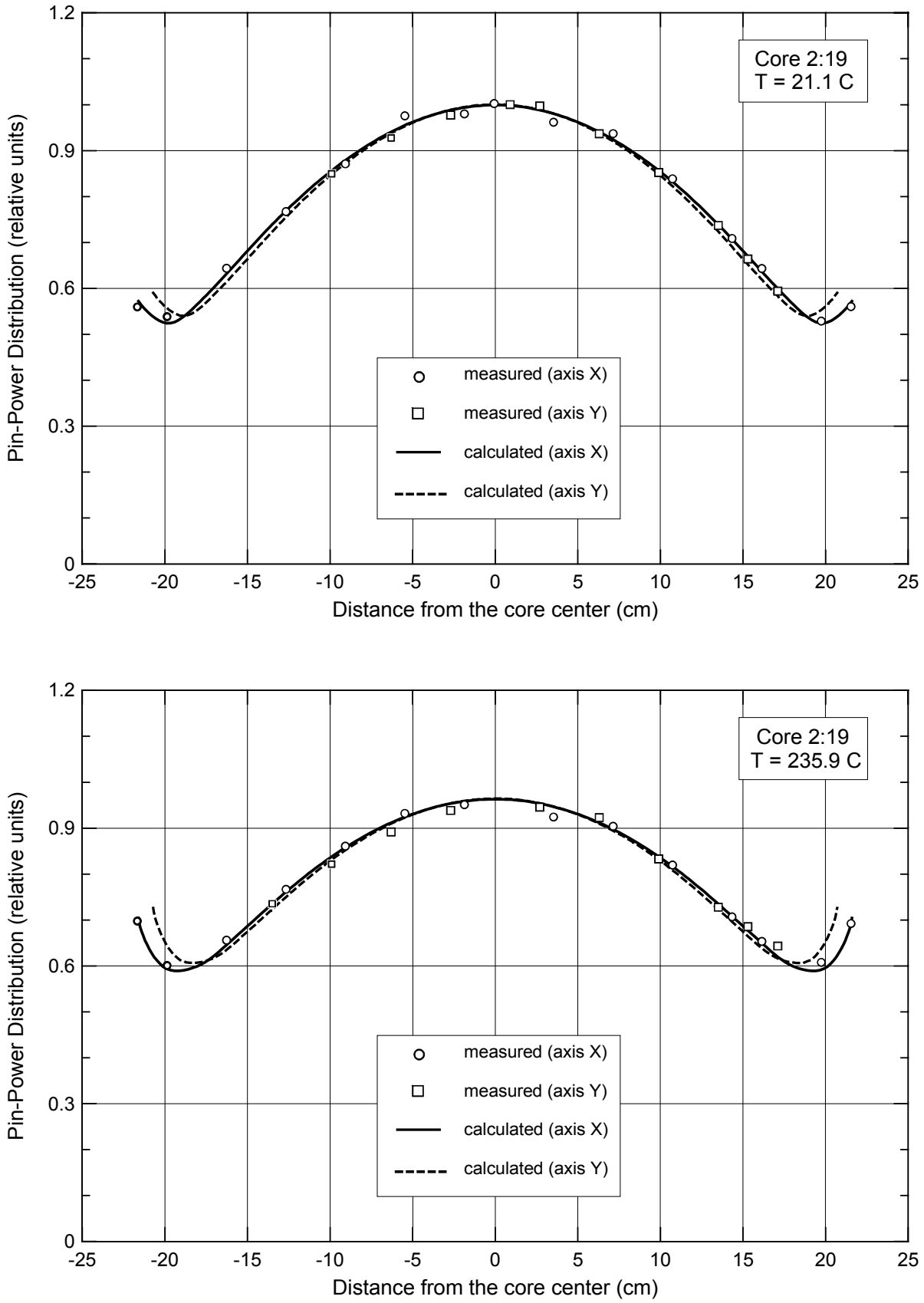

Figure 2.12. Pin-Power Distributions for KRITZ Core 2:19

2.6. UO_2-MOX Core Calculational Benchmark

This core benchmark model has been designed to compare different techniques used for pin-by-pin flux prediction. Detailed specification of the benchmark is given in [17]. Geometry of the benchmark core consists of a 17×17 MOX assembly surrounded by eight 17×17 UO_2 assemblies with 21.42-cm water reflector. The MOX assembly contains fuel pins with 4.3%, 7.0% and 8.7% plutonium enrichments. The UO_2 rods are made of 3.7% enriched in ^{235}U. Vacuum boundary conditions are assumed at the external sides of the reflector. For 2-D calculations, the extrapolated height of the core is 95 cm (axial buckling is $1.094 \cdot 10^{-3}$ cm^{-2}). The temperature is assumed to be constant and equal to 20°C.

The geometries of the UO_2 and MOX assemblies are presented in Figure 2.13 and the core geometry is given in Figure 2.14 where axis X shows a direction for pin power comparison.

In the current comparison with the BARS pin-by-pin calculation, 15 sets of calculational data, obtained by various codes [17], were used. Among them there are two Monte-Carlo codes (MVP and KENO-Va) and one $J_{\pm}$ transport code (ICM2-D). Most of participants used either S_N transport (APOLLO-2, TWOTRAN, TWODANT, and DORT) or diffusion nodal (SILWER, MASTER, PROMETHEUS, NRMPO, and MOSRA) codes.

All participants used different nuclear cross-sections data derived from different libraries (widely spread JEF-2.2, ENDF/B-VI, JENDL-3.2 and FOND-2.2, as well as, the older versions: JEF-1 and MOL-BR2-40GR). The BARS calculations were performed with 5-group database prepared by TRIFON and UNK using ENDF/B-VI based cross-sections. Calculational results for the effective multiplication factor (K_{eff}) are presented in Table 2.17. Here the next column shows deviations in K_{eff} from the mean value (δK_{eff}). The K_{eff} value calculated by DORT (SCK•CEN) is beyond 2σ (approximately 1200 pcm). Practically all the rest results (except for the TWODANT value) are within about 1.5σ. The BARS-TRIFON and BASRS-UNK values, as shown in Table 2.17, are between two APOLLO-2 results.

Comparison of the calculated pin-power distributions was performed in 1/8 core geometry. Note that the report [17] contains an evident misprint in the DORT (SCK•CEN) power data. Table 2.17 presents root-mean-square deviations (RMS) in pin-power distribution relative to the APOLLO-2 (CEA) results as it was done in [17]. It was found that most of the Monte Carlo and transport calculations agreed within a few percent. On the contrary, the diffusion calculations (both nodal and finite-difference), even with the flux reconstruction methods, gave a large discrepancy except for the SILWER code. The last calculation, however, has been performed using the reflector cross-sections adjusted to the known transport solution.

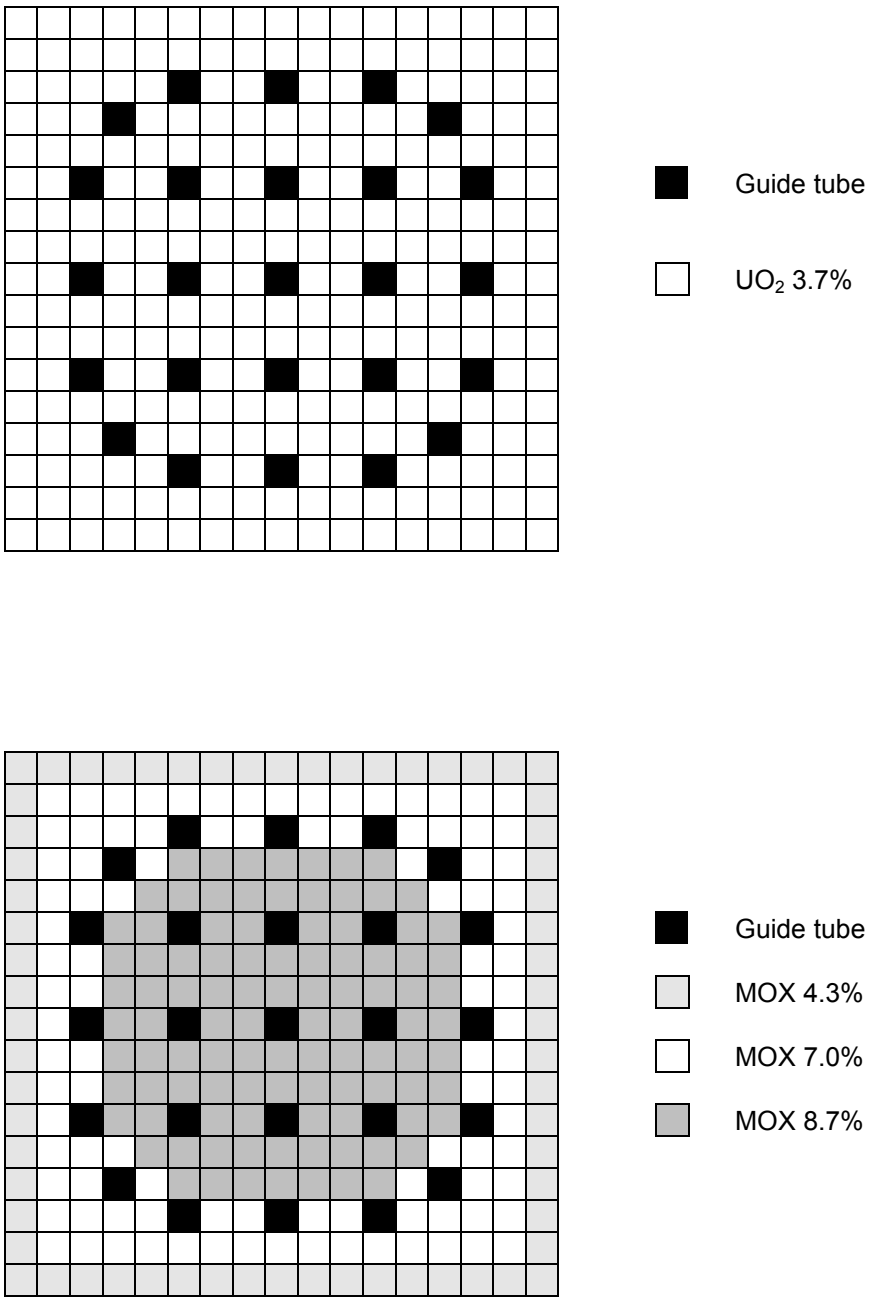

Figure 2.13. Geometry of UO_2 and MOX Assemblies

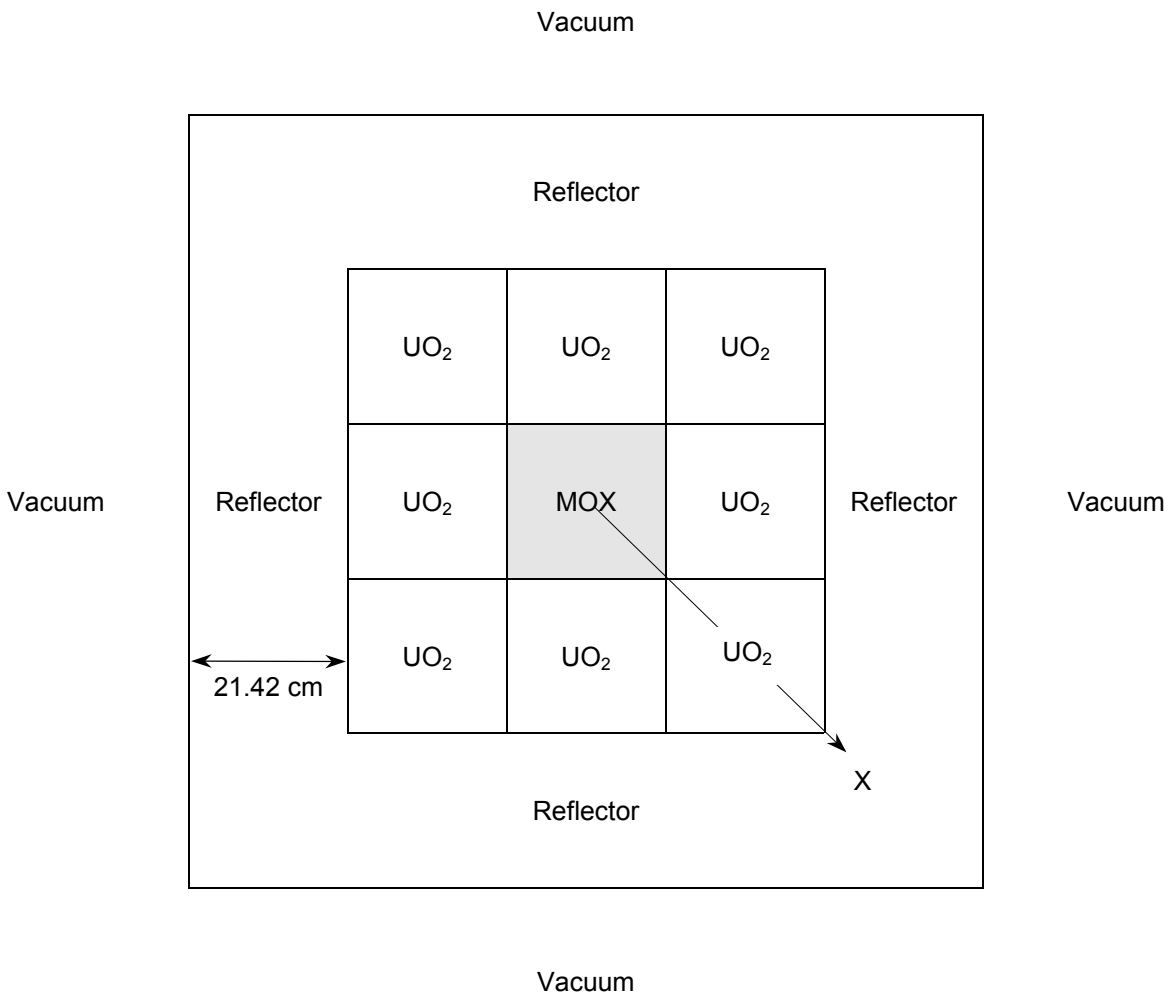

Figure 2.14. Geometry of UO_2-MOX Core

Table 2.17. Comparison of Calculational Results

Method	Code Name (Participant)	K_{eff}	δK_{eff}* (pcm)	RMS (%)	σ_{max} (%)
Transport (S_N or collision probabilities)	APOLLO-2 (CEA)	1.07441	461 (0.43)	-	-
	APOLLO-2 (EDF)	1.07132	152 (0.14)	1.03	-4.8
	TWOTRAN (NRG)	1.06279	-701 (-0.65)	3.20	-9.8
	DORT (Delft)	1.06980	0 (0.00)	0.39	-1.1
	DORT (SCK•CEN)	1.09231**	2104 (2.10)	1.74	5.3
	TWODANT (IPPE)	1.08220	1240 (1.16)	2.02	10.2
$J_{\pm}$ Transport	ICM2-D (IKE)	1.07390	410 (0.38)	0.85	-4.2
Diffusion (nodal or finite-differences)	SILWER (PSI)	1.06996	16 (0.01)	0.65	-2.3
	MASTER (KAERI)	1.06103	-877 (-0.82)	5.39	-21.8
	NRMPO (SCK•CEN)	1.07724	744 (0.69)	7.31	-25.3
	MOSRA (JAERI)	1.06459	-521 (-0.49)	5.09	-26.1
	PROMETHEUS (Delft)	1.06430	-550 (-0.51)	4.03	17.2
	TWODANT (IPPE)	1.06570	-410 (-0.38)	8.83	33.9
Monte Carlo	KENO-Va (Delft)	1.07240	260 (0.24)	1.20	-4.4
	MVP (JAERI)	1.06050	-930 (-0.87)	2.34	9.2
Heterogeneous Theory	BARS-TRIFON (RRC KI)	1.07415	435 (0.41)	2.00	-6.7
	BARS-UNK (RRC KI)	1.07246	266 (0.25)	1.63	-8.1
Mean value of K_{eff} = 1.06980 ± 0.00596					

**In brackets – deviations from the mean value in percents*
***This value was not taken into account to calculate the mean value*

Analysis of the calculated pin-power distributions showed that the maximum deviations (σ_{max} in the last column of Table 2.17) were observed at the corner part of the core, especially for two or three last rows of UO_2 pins. These deviations are both positive and negative: ±10% for the transport and Monte Carlo calculations and about ±30% for the diffusion results. Consequently, RMS deviations vary from 0.9 to 3.2% for the transport and Monte Carlo results and from 4.0 to 8.8% for the diffusion results (except for the SILWER calculation).

It is important to pay attention to the following fact. Separate comparison of the diffusion calculations showed considerably larger discrepancy: RMS deviation and the maximum deviation reached 15 and 80%, respectively. This indicates that certain troubles in cross-sections generation for the core and reflector regions take place for nodal diffusion codes. There is a need to adjust the cross-sections. Such an adjustment procedure includes a comparison with some reference solution obtained by any precise heterogeneous method.

However, in LWR modeling, especially in analysis of reactivity initiated accidents, when the pin-power distribution undergoes considerable local distortions, validation of this adjustment procedure becomes a crucial problem. For instance, as it was shown in [18], the adjustment parameters (or flux discontinuity factors) for the reflector region are sensitive not only to a calculational method and the core conditions, but also to a node position. In other words, the adjustment parameters of different nodes in the reflector region differ from each other. So, it is difficult to expect that a variety of possible conditions can be involved in such a way. As a result, the drawbacks of a nodal diffusion method may lead to noticeable uncertainties in important safety-related parameters.

As Table 2.17 shows, the BARS results are in very good agreement with the APOLLO-2 (CEA) calculation. Comparison with other calculations is given in Table 2.18. Four transport results and both Monte Carlo results (KENO-Va and MVP) were selected to compare with the BARS calculations. This table shows root-mean-square deviations (RMS) in pin-power distributions between the BARS and the selected codes. Figure 2.15 shows the relative pin-power distributions (along axis X as shown in Figure 2.14) calculated by the BARS-UNK, APOLLO-2 (CEA), ICM2-D, and KENO-Va codes. The maximum deviations between BARS and other codes were found for the last row of UO_2 pins near the core-reflector interface.

Table 2.18. RMS Deviations (%) in Pin-Power Distribution

	APOLLO-2 (EDF)	DORT (Delft)	DORT (SCK•CEN)	ICM2-D (IKE)	KENO-Va (Delft)	MVP (JAERI)
BARS-TRIFON	1.87	2.03	1.05	1.76	1.81	3.43
BARS-UNK	1.18	1.53	1.55	1.12	1.21	2.91

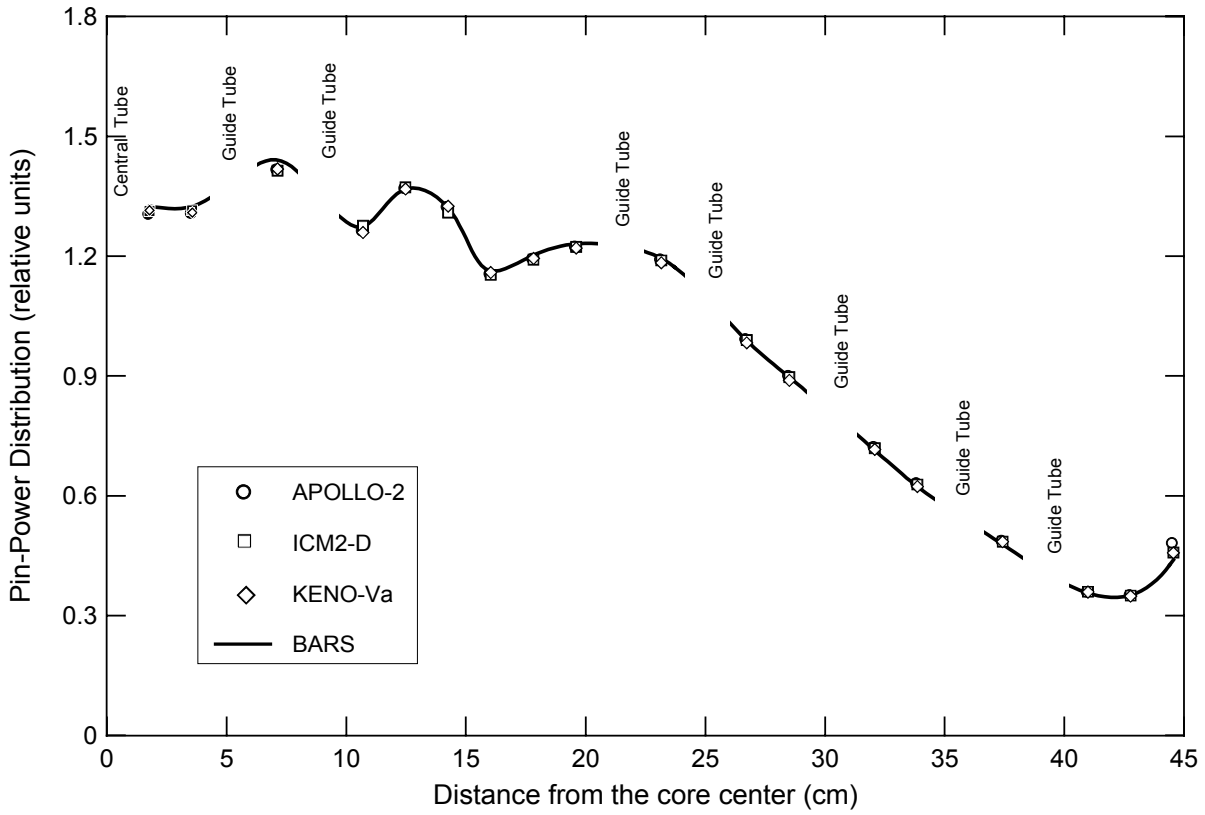

Figure 2.15. Comparison of Pin-Power Distributions

2.7. Discussions

Analysis of the BARS calculational results for five experimental and one numerical core benchmarks shows the following:

- An uncertainty in K_{eff} calculation practically do not depend on which database was used: generated by TRIFON or UNK. The mean value of K_{eff} are (for the TRIFON and UNK databases):

  - PNL MOX cores - 0.9972 ± 0.0050 and 0.9958 ± 0.0048;
  - Saxton MOX cores - 0.9885 ± 0.0034 and 0.9880 ± 0.0021;
  - TCA MOX cores - 0.9899 ± 0.0031 and 0.9903 ± 0.0033;
  - ESADA MOX cores - 0.9984 ± 0.0046 and 0.9969 ± 0.0044;
  - KRITZ MOX cores - 0.9927 ± 0.0026 and 0.9929 ± 0.0027.

  Thus, BARS underestimates the K_{eff} value for the Saxton and TCA MOX cores by 1%; on average, BARS underestimates the K_{eff} value by about 0.5%.

- Pin-power distributions calculated by BARS using two databases (generated by TRIFON or UNK) agree with rather high accuracy with the experimental or calculated by Monte Carlo or S_N methods. The average root-mean square deviations are as follows (for the TRIFON and UNK databases):

  - PNL MOX cores - 1.47% and 1.44% (as compared with the measurements);
  - PNL MOX cores - 1.19% and 1.00% (as compared with the KENO-V data);
  - Saxton MOX cores - 1.25% and 0.97% (as compared with the KENO-V data);
  - TCA MOX cores - 1.34% and 1.10% (as compared with the KENO-V data);
  - KRITZ MOX cores - 1.51% and 1.38% (as compared with the measurements);
  - UO_2-MOX core - 1.87% and 1.18% (as compared with the APOLLO data);
  - UO_2-MOX core - 1.05% and 1.55% (as compared with the DORT data).
  - UO_2-MOX core - 1.81% and 1.21% (as compared with the KENO-V data).

  Thus, the BARS calculations with the UNK database give lower uncertainties in the pin-power distribution in comparison with the results obtained with the TRIFON database.

References

1. R. I. Smith and G. J. Konzek, “Clean Critical Experiment Benchmarks for Plutonium Recycle in LWRs,” EPRI-NP-196, Vol.1, April 1976
2. R. I. Smith and G. J. Konzek, “Clean Critical Experiment Benchmarks for Plutonium Recycle in LWRs,” EPRI-NP-196, Vol.2, September 1978
3. International Handbook of Evaluated Criticality Safety Benchmark Experiments, “MIX-COMP-THERM-002 Benchmark. Rectangular Arrays of Water-Moderated UO_2-2 wt.% PuO_2 (8% ^{240}Pu) Fuel Rods,” NEA/NSC/DOC/(95)03/VI, Volume VI, September 2001
4. D. F. Hollenbach and P. B. Fox, “Neutronics Benchmarks of Mixed-Oxide Fuels Using the SCALE/CENTRM Sequence,” ORNL/TM-1999/299, February 2000
5. R. D. Mosteller, “Two-dimensional Benchmark Calculations for PNL-30 Through PNL-35,” Trans. Am. Nucl. Soc., **77**, p.371, 1997
6. W. Bernnat et al., “Analysis of LWR Benchmarks Based on Different Methods and Nuclear Data Evaluations,” Proceedings of the ANS International Topical Meeting on Advances in Reactor Physics and Mathematics and Computation into the Next Millenium (PHYSOR-2000), Pittsburgh, Pennsylvania, USA, May 7-12, 2000
7. International Handbook of Evaluated Criticality Safety Benchmark Experiments, “MIX-COMP-THERM-003 Benchmark. Rectangular Arrays of Water-Moderated UO_2-6.6 wt.% PuO_2 Fuel Rods,” NEA/NSC/DOC/(95)03/VI, Volume VI, September 2001
8. N. M. Abdurrahman, G. Radulescu and I.Carron, “Benchmark Calculations of the Saxton Plutonium Program Critical Experiments,” Nuclear Technology, **127**, p.315, September 1999
9. G. F. Cuevas Vivas and T. Parish, “Analyses of the Saxton Plutonium Criticals Using WIMSD4M and DIF3D,” Trans. Am. Nucl. Soc., **77**, p.367, 1997
10. G. F. Cuevas Vivas and T. Parish, “MOX Use in Reactors: Benchmarking of Neutronic Codes. Analyses of Selected Saxton Plutonium Program Experiments Using WIMS7a,” ANRCP-1999-12, March 1999
11. International Handbook of Evaluated Criticality Safety Benchmark Experiments, “MIX-COMP-THERM-004 Benchmark. Critical Arrays of Plutonium-Uranium Fuel Rods with Water-to-Fuel Volume Ratios Ranging from 2.4 to 5.6,” NEA/NSC/DOC/(95)03/VI, Volume VI, September 2001

12. R. D. Leamer et al., “PuO_2-UO_2 Fueled Critical Experiments,” Westinghouse Electric Corp., WCAP-3726-1, July 1967

13. H. Akkurt and N. M. Abdurrahman, “Neutronics Benchmarks for the Utilization of Mixed-Oxide Fuel: Joint U.S./Russian Progress Report for Fiscal Year 1997. Volume 4, Part 5 - ESADA Plutonium Program Critical Experiments: Multiregion Core Configurations,” ORNL/SUB/00-XSZ175V-1, February 2000

14. H. Akkurt and N. M. Abdurrahman, “Benchmark Calculations of the ESADA Single-Region Mixed-Oxide Critical Experiments,” Nuclear Technology, **127**, p.301, September 1999

15. N. M. Abdurrahman and H. Akkurt, “Criticality Benchmark Calculations of the ESADA Plutonium Program Experiments with MCNP,” Trans. Am. Nucl. Soc., **77**, p.368, 1997

16. E. Johansson, “Data and Results for KRITZ Experiments on Regular H_2O/Fuel Pin Lattices at Temperatures up to 245 C,” STUDSVIK/NS-90/133, November 1990

17. “Benchmark Calculations of Power Distribution within Fuel Assemblies. Phase II: Comparison of Data Reduction and Power Reconstruction Methods in Production Codes,” NEA/NSC/DOC(2000)3, November 2000

18. Y. Tahara, T. Kanagawa and H. Sekimoto, “Two-Dimensional Baffle/Reflector Constants for Nodal Code in PWR Core Design,” Journal of Nuclear Science and Technology, **37**, No.11, p.986-995, November 2000

CONCLUSIONS

Growing interest in large-scale use of MOX fuel in LWRs, engenders a need to improve calculational tools used for the in-core management and safety analysis of nuclear reactors with UO_2 fuel. During past few decades, several countries accumulated rich experience in reusing of MOX fuel recovered from spent fuel. However, main neutronic parameters for MOX-fuelled cores differ from those for UO_2 fuel cores. Numerous estimations showed that different isotopic and spectral characteristics of MOX fuel compared with UO_2 fuel, result in lower boron and control rod worth and more negative fuel and moderator temperature coefficients. Thus, problems of improvements in approaches for modeling MOX cores and corresponding validation procedures become essential.

This report is focused on the BARS code package validation for MOX-fuelled systems. All calculational results were obtained using the neutron databases generated on the basis of the nuclear evaluated file ENDF/B-VI by either the TRIFON or UNK codes.

The pin cell modeling was used to validate a procedure to generate neutron database by the TRIFON or UNK codes. A number of different MOX fuel cells with various compositions and geometries were considered. The following important parameters were investigated: the multiplication factor, neutron balance, and the reactivity effects. The last effects include the fuel temperature (Doppler) effects, the void and moderator temperature effects, and the boron and Xe/Sm poisoning effects. Comparisons were carried out using the calculational results obtained by using modern codes (based on Monte Carlo or transport methods) with most advanced nuclear libraries, such as ENDF/B-V, ENDF/B-VI, JEF-2.2, and JENDL-3.2. It was found that uncertainties in the MOX cell parameters are, as a rule, higher compared with those for UO_2 cells. It is necessary to use advanced methods for plutonium resonance treatment, as well as increased number of energy groups in the neutron libraries. Besides, it turned out that the Monte Carlo calculation did not guarantee a better result. Apparently, there is a need for more careful preparation of the neutron database used for the MOX fuel calculations by both Monte Carlo and transport codes.

Both TRIFON and UNK demonstrate rather good agreement in calculations of K_{inf}, neutron balance, and the reactivity effects in the MOX fuel cells. The reactivity effects, such as the Doppler, moderator temperature, and the boron or Xe/Sm poisoning effects are calculated within 5% uncertainty. The void effect up to 70% void fraction is predicted with 5-10% uncertainty. The UNK results are very close to the mean values and, therefore, the UNK code is more preferable in the MOX fuel calculations.

The spatial pin-by-pin power effects were investigated within rather simple MOX-fuelled cores of LWR type. Both the experimental and numerical benchmark cores were used. The effective multiplication factor and power distribution inside the core were compared with the measurements and calculational results obtained by using different codes. It was found that the BARS code underestimates the K_{eff} value for the Saxton and TCA MOX cores by 1%; on average, BARS underestimates K_{eff} by about 0.5%. There is no noticeable difference between the BARS-TRIFON and BARS-UNK calculations.

Pin-power distributions calculated by BARS using two databases (generated by TRIFON or UNK) agree with rather high accuracy with the experimental or calculated by Monte Carlo or S_N methods. The average root-mean square deviations do not exceed 1.9% and 1.5% for the BARS-TRIFON and BARS-UNK calculations, respectively. These deviations are of the same order as it was found during previous validation for simple UO_2-assemblies [1]. As in case of the MOX pin cell calculations, it is safe to notice that the UNK code is preferable in calculations of the MOX fuelled cores.

It should be mentioned that unlike S_N or, especially, Monte Carlo methods, a heterogeneous method implemented in BARS is fast-running. This advantage allows successfully to use the BARS code for LWR full-scale calculations including modeling of various transients with quite reasonable computational costs.

Nowadays nodal diffusion methods are mainly used for most LWR design purposes and widely spread all around. But, as it was found in benchmark calculations of a very simple model of a PWR containing MOX fuel, these methods need a special adjustment procedure for the cross-sections. As reported in [2], in comparison with the transport or Monte Carlo calculations the diffusion calculations gave a large discrepancy in the pin-power distribution, especially near the core-reflector interface (more than 30%). Moreover, single comparison of the nodal diffusion calculations showed considerably larger discrepancy (up to 80%). This indicates very poor accuracy in prediction of the pin-power effects.

It seems reasonable to conclude from above validation results that the BARS code package can be used in calculations of MOX-fuelled LWR with a precision adequate for most design purposes. The BARS code package allows to predict all basic safety-related parameters of MOX fuel. The BARS validation results demonstrate very good accuracy in prediction of the pin-power effects in the cores containing both UO_2 and MOX fuels.

References

1. Avvakumov, et al., “Validation of the BARS Code Package with ENDF/B Based Data Library,” Report No. 90-12/1-4-98, Nuclear Safety Institute of Russian Research Centre “Kurchatov Institute”, 1998
2. “Benchmark Calculations of Power Distribution within Fuel Assemblies. Phase II: Comparison of Data Reduction and Power Reconstruction Methods in Production Codes,” NEA/NSC/DOC(2000)3, November 2000